Journal of Hydrology 625 (2023) 130012

Contents lists available at ScienceDirect

Journal of Hydrology

journal homepage: www.elsevier.com/locate/jhydrol

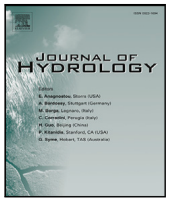

Research papers

On the relation between antecedent basin conditions and runoff coefficient for European floods

Christian Massari [a,*], Victor Pellet [b,j], Yves Tramblay [c], Wade T. Crow [d], Gaby J. Gründemann [e], Tristian Hascoetf [f], Daniele Penna [g,a], Sara Modanesi [a], Luca Brocca [a], Stefania Camici [a], Francesco Marra [h,i]

[a] Research Institute for Geo-Hydrological Protection, National Research Council, Perugia, Italy
[b] Laboratoire d'Etudes du Rayonnement et de la Matière en Astrophysique et Atmosphères, (LERMA), Observatoire de Paris, Observatoire de Paris, Paris, France
[c] HSM, Univ. Montpellier, CNRS, IRD, Montpellier, France
[d] Hydrology and Remote Sensing Laboratory, USDA ARS, Beltsville, MD, US
[e] Department of Water Management, Delft University of Technology, Delft, The Netherlands
[f] Graduate School of System Informatics, Kobe University, Kobe, Japan
[g] Department of Agriculture, Food, Environment and Forestry (DAGRI) University of Florence, Florence, Italy
[h] Department of Geosciences, University of Padova, Padova, Italy
[i] Institute of Atmospheric Sciences and Climate, National Research Council (CNR-ISAC), Bologna, Italy
[j] ESTELLUS, Paris, France

ARTICLE INFO

This manuscript was handled by Marco Borga, Editor-in-Chief.

MSC:
49027

Keywords:
Floods
Runoff coefficient
Precipitation

ABSTRACT

The event runoff coefficient (i.e. the ratio between event runoff and precipitation that originated the runoff) is a key factor for understanding basin response to precipitation events. Runoff coefficient depends on precipitation intensity and duration but also on specific basin geohydrology attributes (including soil type, geology, land cover, topography) and last but not least, antecedent (or pre-storm) conditions (i.e., the amount of water stored in the different hydrological compartments, like the river, groundwater, soil and snowpack). The relation between runoff coefficient and basin pre-storm conditions is critical for flood forecasting, yet, the understanding of where, when and how much basin pre-storm conditions control runoff coefficients is still an open question.

Here, we tested the control of basin pre-storm conditions on runoff coefficient for 60620 flood events across 284 basins in Europe. To do so, we derived basin pre-storm conditions from different proxies, namely: antecedent precipitation; surface and root zone soil moisture from hydrological models, reanalyses and land surface models also ingesting satellite observations; pre-storm river discharge, and pre-storm total water storage anomalies. We evaluated the coupling strength between runoff coefficient and pre-storm conditions proxies in relation to five classes of European basins, defined based on land use and soil type (as indexed by the Soil Conservation Service curve number *CN*), topography, hydrology and long-term climate and tested their ability to explain stormflow volume variability.

We found that precipitation explains relatively well the stormflow volumes for both small and large events but not very well the peak discharge, especially for large floods. The runoff coefficient of events shows different distributions for the five different classes and correlates well with deep soil storages (such as root-zone soil moisture and pre-storm total water storage anomalies), pre-storm river discharge, and pre-storm snow water equivalent. Overall, these correlations depend on the class. Poor correlations are found against antecedent precipitation index despite its wide use in the hydrological community. Seasonal and interannual climate variability exert a key role on the coupling strength between runoff coefficient and pre-storm conditions by inducing sharp changes in the correlation with season and climate.

These results increase our understanding of the coupling between pre-storm conditions and runoff coefficients. This will aid flood forecasting, hydrological and land surface model calibration, and data assimilation. Furthermore, these findings can help us to better interpret future flood projections in Europe based on expected changes in long and short-term climatic drivers.

* Corresponding author.
E-mail address: christian.massari@irpi.cnr.it (C. Massari).

https://doi.org/10.1016/j.jhydrol.2023.130012
Received 26 October 2022; Received in revised form 31 May 2023; Accepted 1 August 2023
Available online 21 August 2023

1. Introduction

In addition to its exceptional total rainfall, the devastating flood that impacted Germany, Belgium, Luxembourg and other neighboring countries in July 2021 and Emilia Romagna (Italy) in 2023 was amplified by abundant precipitation during the weeks preceding the event. This brought the pre-storm soil moisture conditions of the affected basins very close to saturation, and actively contributed to the extreme river discharges and flood volume observed at many sites (https://www.eumetsat.int/devastating-floods-western-europe, https://en.wikipedia.org/wiki/2023_Emilia-Romagna_floods). Indeed, "extreme" precipitation intensity and amount are not necessarily the sole cause of extreme flooding (Ivancic and Shaw, 2015; Sharma et al., 2018; Wasko et al., 2020) as basin pre-storm conditions modulate the basin response to precipitation (Tramblay et al., 2010). Climate change is expected to increase the magnitude of extreme precipitation events (Gründemann et al., 2022) and, at the same time, alter the interplay between wet and dry spells (Vaittinada Ayar and Mailhot, 2021; Zolina et al., 2013). It will, therefore, modify soil moisture conditions in complex ways. A correct representation of the link between pre-storm conditions and basin response by models is therefore critical for future flood and flood-risk projections (Chen et al., 2011; Sharma et al., 2018). However, the actual limits of models to represent soil moisture and the link between pre-storm soil moisture and runoff challenges our ability to predict the streamflow generated by future precipitation events (Crow et al., 2019).

Runoff coefficient (*RC*), defined as the ratio between the stormflow volume (i.e., stormflow) and the rainfall that produced the flood, quantifies the amount of precipitation that is transformed into runoff. *RC*, thus, it depends both upon the water stored in the soil, river, and groundwater prior to the rainfall event (i.e., pre-storm wetness conditions or simply "pre-storm conditions" hereinafter), and on a number of factors including land cover, topography, soil type, and specific basin hydrology (normally described by hydrological signatures). Therefore, accurately characterizing and anticipating *RC* is crucial in flood forecasting. As the actual *RC* can only be computed after a flood has occurred, flood forecasting and early-warning systems need to understand how the above-mentioned variables (that are usually known before the flood event) are linked to the *RC* of the subsequent event (that is only known after the event).

Given its dependence upon multiple factors, *RC* is characterized by high variability in both space and time (Viglione et al., 2009; Norbiato et al., 2009; Merz and Blöschl, 2009; Penna et al., 2013; Wu et al., 2021). Evidence suggests that pre-storm conditions, and soil saturation in particular, exert a key role in determining the land-surface response to extreme precipitation at different basin scales (Norbiato et al., 2009; Merz and Blöschl, 2009; Marchi et al., 2010; Penna et al., 2011, 2016; Berghuijs et al., 2019; Bertola et al., 2021). In particular, Berghuijs et al. (2019) found that floods in Europe are almost exclusively driven by soil moisture excess and thus high antecedent soil moisture values may result in a more severe response to precipitation. The importance of this generation process was found by the same authors to exceed that of the other processes like snowmelt and extreme precipitation combined.

The important role of antecedent conditions as a dominant control on the spatiotemporal variability of event runoff coefficients was shown by Merz and Blöschl (2009), who investigated how *RC* varies as a function of climate forcing, geology, soil types and land use over a large set of Austrian basins. Similarly, Guastini et al. (2019) illustrated how *RC* varies as a function of the basin scale (0.14–109 km^2). Tarasova et al. (2018) also indicated that, unlike antecedent soil moisture and pre-event baseflow, antecedent precipitation indices do not accurately represent the wetness state of German basins. Storm-to-storm variations in pre-storm soil moisture (i.e., pre-storm soil moisture change from event to event) was also found to be a good proxy for *RC* across the Mediterranean area and beyond (see Brocca et al., 2009; Tramblay et al., 2010, and references therein).

Soil moisture is normally derived from hydrological and land surface models, satellite observations or in situ measurement networks and then can significantly vary in terms of its vertical and spatial support as well as in its dynamic. For instance, soil moisture information is available from different soil parameterizations found within land surface and hydrological models (Zhao et al., 2019). Satellite surface soil moisture observations depend on the type of sensors (Kim et al., 2019) and, depending on the retrieval band, they can be representative of different depths. Alternatively, pre-storm conditions can be obtained from river discharge and antecedent precipitation indices (*API* Ponce and Hawkins, 1996), which can be used as a soil moisture index. These pre-storm condition proxies are used in many operational applications.

At the time of writing, the increased availability of soil moisture indices of varying vertical supports (i.e., representing different soil depth and thus different soil storages) offer additional alternatives to support flood forecasting. These include satellite estimates of surface soil moisture (Bauer-Marschallinger et al., 2019; Entekhabi et al., 2010; Kerr et al., 2001), root-zone soil moisture derived from a combination of models and satellite observations (Manfreda et al., 2014; Martens et al., 2017; Reichle et al., 2017) and relatively new terrestrial water storage anomaly estimates obtained from satellite gravimetric missions (Tapley et al., 2004). This information can be utilized, for instance, via data assimilation into land surface and hydrological models (Kumar et al., 2009; Mao et al., 2020; De Santis et al., 2021; Lievens et al., 2015), initialization of event-based rainfall-runoff models (Massari et al., 2014; Mahdi El Khalki et al., 2020), flood forecasting via machine learning approaches (Rasheed et al., 2022), or by the direct integration of these products into operational applications, e.g., the flash flood guidance system operated by NOAA https://www.weather.gov/serfc/ffg.

The success of the use of these products in flood forecasting, however, eventually depends on how strongly antecedent conditions are coupled with runoff response, and thus on how much these products are able to represent the link between antecedent conditions and *RC*. In other words, it depends on the extent to which they can predict how much precipitation will be transformed into stormflow. This not only depends on their relative accuracy or representativeness but also on basin characteristics and climate as underlined above. Nonetheless, the coupling strength between antecedent conditions and *RC* is critical in data assimilation experiments for improving streamflow predictions (Chen et al., 2011; Massari et al., 2014; Lievens et al., 2015; Baugh et al., 2020; Mao et al., 2020; Betchold et al., 2023), in data calibration and initialization of rainfall-runoff model (Shahrban et al., 2018; Mahdi El Khalki et al., 2020), and for understanding the potential of future floods (Reager and Famiglietti, 2009; Sharma et al., 2018). For instance, in large data assimilation studies aiming at improving streamflow simulations, diverse attempts to ingest satellite surface soil moisture retrievals (Chen et al., 2011; Kumar et al., 2009; De Santis et al., 2021) led to inconclusive results. De Santis et al. (2021), for example, showed that the assimilation of surface soil moisture satellite observations over cold and humid climate did not bring any added benefit and, in fact, partially deteriorated the ability of the models to predict runoff under certain conditions.

Therefore, understanding the degree to which specific pre-storm condition proxies are coupled to *RC*, and the impact of basin characteristics (i.e., climate, season, location, topography, land cover and basin specific hydrology) on such coupling, is crucial in flood research and applications. The answer to this specific question has been explored often for individual basins or at a local/regional level (see references above), but – to our knowledge – has never been examined using an integrated approach considering multiple basins spanning different climates and basin characteristics.

In this study, we analyze the role of pre-strom proxies in modulating *RC* and explain stormflow volume variability. To do so, we compare different basin pre-storm indices (e.g., *API*, pre-storm river discharge, surface and root-zone soil moisture, as well as total water storage anomalies, *TWSA*, coming from hydrological models, reanalysis data

and land surface models ingesting satellite soil moisture observations) to explain observed *RC* variability across historical European floods. We consider the impact of climate, season, land cover, topography, and the hydrological signatures of the basins and use correlation and regression analyses and datasets of precipitation and river discharge observations (1980–2015) from 284 basins across Europe, from which we extracted more than 60000 flood events. This work goes beyond the analysis of Crow et al. (2017) and Massari and Camici (2020) as it considers the effect of the climate and basin type on the coupling strength between these variables and *RC*. Furthermore, it uses longer time records of precipitation and river discharge — which allow us to focus on an adequate sample of "true" flood events.

2. Study area and dataset

2.1. Study area and basin characteristics

The examined 284 basins result from the stringent screening process of more than 3900 stations across Europe (see below) and range between 507 and 19920 km^2 in size (see Figure SI 2). This is a range of areas similar to the one used by other studies (Merz and Blöschl, 2009) and guarantees relatively small uncertainty due to the spatial interpolation of rainfall (for smaller basins) and the small spatial variability of *RC* (for larger basins). The basin selection was carried out with the aim of maximizing the geographical coverage and the long-term availability of daily streamflow records (i.e., from 1980 to 2015 at least) collected from the Global Runoff Data Center (GRDC, https://www.bafg.de/GRDC/EN/01_GRDC/grdc_node.html). The selected basins passed a careful quality control aimed at excluding stations with unreliable time series due to human regulations (e.g., unrealistically constant flows), inhomogeneity, or problems in the low-flow range (as suggested in Kundzewicz and Robson (2004).

2.2. Precipitation, soil moisture, evaporation products and ancillary datasets

Precipitation, temperature, and snow water equivalent (*SWE*) data used in this study were obtained from the ERA5 reanalysis dataset (Hersbach et al., 2020). ERA5 is particularly suitable for this study due to its homogeneity, demonstrably good performance over Europe (Bandhauer et al., 2021), and permissive usage license (Anon, 2020). We acquired ERA5 data from 1979–2019 at a 0.25° (about 30 km) resolution for an hourly time step and summed them to obtain daily estimates.

Soil moisture data were obtained from the following reanalysis, hydrological models, and remote sensing observations:

1. ERA5 reanalysis (1979–2019, 0.25°) over three soil layers: 0–7 cm, 7–28 cm and 28–100 cm. These data were acquired at an hourly timestep and averaged to obtain daily data. In an evaluation study using 25 soil moisture networks including those in Europe, ERA5 was shown to be superior to other reanalysis datasets (Li et al., 2020).
2. Sacramento hydrological Model (SAC) surface and root zone soil moisture obtained via the calibration of the SAC model against observed streamflow time series. We used ERA5 precipitation and temperature for calculating potential evaporation via the Haymon formulation (Lu et al., 2005). SAC model has been used extensively for operational stream flow forecasting within medium-sized (about 1000 km^2) river basins (Burnash, 1995). Soil moisture accounting in the model is based on the estimation of different soil water states: upper-zone free water content ($UZFWC$), upper-zone tension water content ($UZTWC$), lower-zone tension water content ($LZTWC$), lower-zone free primary water content ($LZFPC$), and lower-zone free supplemental water content ($LZFSC$) which we combined to obtain basin-scale surface and root zone soil moisture ($SSM_{SAC} = UZFWC+UZTWC, RZ_{SAC} = LZFPC+LZTWC+LZFSC$). Details related to the calibration and application of the SAC model to the basins are reported in the supplementary material. We found comparable river discharge simulation performance to other model studies in Europe based on similar forcing datasets (Camici et al., 2018; De Santis et al., 2021). Note that, being a conceptual model, SAC does not assign specific surface and root zone specific depths to its soil moisture states.
3. The Global Land Evaporation Amsterdam Model (GLEAM, Martens et al., 2017). This is a suite of algorithms that separately estimate different components of the terrestrial evaporation by using data from satellite observations and atmospheric reanalyses. The model uses the Priestley and Taylor equation to estimate potential evaporation, and combines global satellite observations – mostly derived from microwave observations – to estimate different evaporation components via an evaporative stress factor. Surface and root-zone soil moisture are calculated using a multi-layer running water balance model that uses observed precipitation as an input and the assimilation of satellite soil moisture observations. Here we used the GLEAM version 3.5a which ingests ESA-CCI soil moisture observations to obtain basin-scale daily evaporation, surface (0–10 cm, SSM_{GLEAM}) and root-zone (10–100 cm, RZ_{GLEAM}) soil moisture estimates. Despite being based on a combination of model and remote sensing information, GLEAM is based on satellite observations and is therefore assumed here to be representative of satellite soil moisture datasets such as the SMAP Level 2 and 3 products — with quasi-daily temporal resolution that only cover the period after 2015 (note that CCI soil moisture is available since 1979, but it is not usable here due to its noticeable number of missing values prior to 2001).

Other ancillary data were collected to describe the relatively static basin attributes (Fig. 1):

1. Land cover and soil texture as indexed by the curve number (*CN*). *CN* was estimated by using the dataset of Hong et al. (2007) extracted from the MODIS land cover classification and the hydrological soil group map are used to estimate the *CN* by indexing in the standard lookup tables of the Natural Resources Conservation Service Ponce and Hawkins, 1996.
2. Topography. Topographic complexity (*tc*) and elevation (*elev*) were calculated on GTOPO30 digital elevation model. In particular, *tc* was quantified by the standard deviation of DEM cells contained in the basin.
3. Aridity index (*AI*) calculated as the ratio between long-term mean annual potential evaporation and mean annual precipitation both from ERA5 data.
4. Hydrological behavior via hydrological signatures. Three different hydrological signatures were considered and computed using the Gnann et al. (2021) toolbox: (i) the Base Flow index (*bfi*), that is the ratio between baseflow (volume) and total streamflow (volume), (ii) the Richard–Baker Flashiness index (*fl*), that quantifies the response time of runoff after the onset of a rainfall event and the subsequent return to base flow conditions (Baker et al., 2004) and (iii) the Variability Index (*vi*), that is the standard deviation of the common logarithms of discharge determined at 10% intervals from 10% to 90% of the cumulative frequency distribution.

Fig. 1 reveals a clear climate pattern with more water limited basins ($AI > 1$) located in central and eastern Spain and more energy limited ones over northern latitudes and across the mountainous regions. Basins in the transition between fully water limited and fully energy limited are located over the Western Iberia peninsula, Southern France, Eastern Europe, and Southern UK. From the figure, basins located in

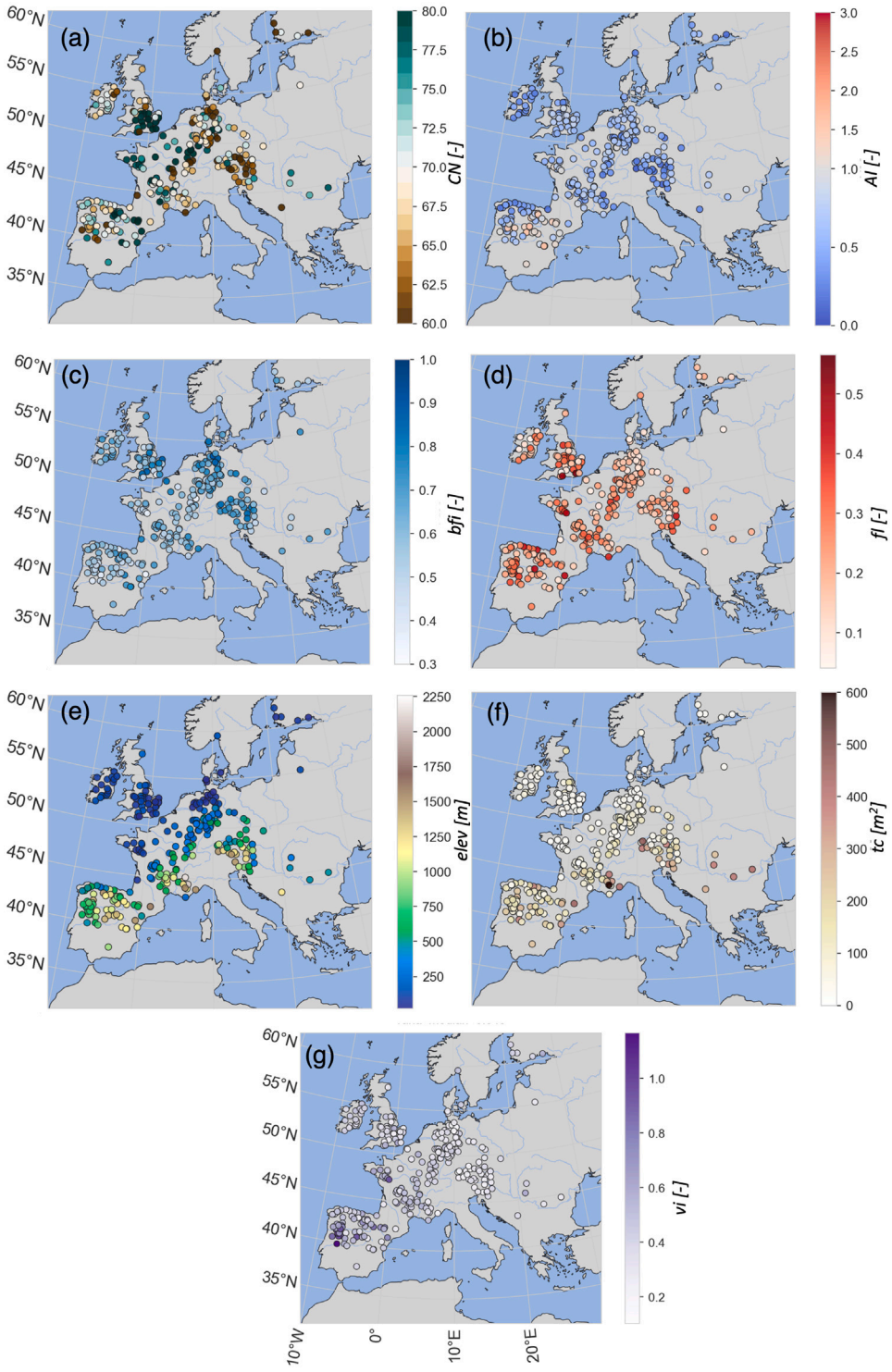

Fig. 1. Static attributes characterizing basins. (a) land cover as indexed by curve number (*CN*), (b) Aridity Index (*AI* = *PET/precipitation*) derived from long term potential evapotranspiration and precipitation, (c) baseflow index (*bfi*) based on the Lyne and Hollick baseflow separation method, (d) flashiness (*fl*), (e) elevation, (f) topographic complexity (*tc*), (g) variability (*vi*). For each feature, the median value is given in the title of the figures.

Southern Europe are also characterized by higher elevation and more complex topography. There is not a clear pattern between *CN*, *bfi* and *fl*.

3. Methods

3.1. Flood event extraction

Flood event extraction was carried out by the following steps:

1. We separated the stormflow from the baseflow using the method of Hewlett and Hibbert (1967) also credited by McDonnell (2009). In this method, the flood extraction is done using an algorithm that relies on two parameters: the area of the catchment Ab and a parameter k that controls the slope of the dividing line, that is, the slope that defines when event water separates from the baseflow. k was set equal to 0.000546 m^3 s^{-1} km^{-2} d^{-1} as suggested by McDonnell (2009) which provided the most reasonable flood event separation (visually). This was further confirmed by carrying out the analysis with different k values (using for k values equal to $\frac{0.000546}{n}$ with $n = [-10, +10]$ excluding zero. $k = 0.000546$ was the one providing the best agreement (i.e., Pearson correlation coefficient) between event runoff coefficients and antecedent condition proxies. The tests with different k values showed a low sensitivity to the magnitude of k itself. The source code of the function to separate event water from runoff is freely distributed via https://hydrograph-py.readthedocs.io/en/latest/index.html.
2. To distinguish between two close flood events we calculated for each basin the concentration time Tc as: $Tc = L/0.6$ with $L = 1.19Ab^{0.33}$ representing the lag time for the basin and Ab the basin area as proposed by Melone et al. (2002). The coefficient (1/0.6) was derived from the formulation of the concentration time as proposed by Simas (1996), that can be assumed valid for natural basin conditions given an approximately uniform spatial distribution of runoff.
3. To select the onset of the event (when precipitation that produces the flood begins) we used the precipitation accumulated in the previous Tc days (API_{Tc}). In particular, starting from the presence of stormflow in the river identified at point 1 we considered N time steps backward until API_{Tc} was found lower than 2 mm. The satisfaction of this condition marks the beginning of the flood event. The event was considered to end when the stormflow was equal to zero.
4. Events with *RC* larger than 2 were excluded to remove potential errors in the data (these events were less than 0.1%, though, so they did not impact the analysis).

The so applied flood event extraction resulted in 60620 separate flood events. An example of the event separation is reported in the supplementary material in Figure SI 1 along with the percentage of flood events with *RC* larger than one for the different seasons and different classes (see Figures SI 3 and SI 4) that resulted in about 2.5% at maximum.

3.2. Pre-storm condition proxies

We considered several proxies for the pre-storm conditions:

1. The five days antecedent precipitation index (*API5*, Kohler, 1951, *API* from here onward), which aims at reproducing the saturation state of the basin prior to the event by calculating the cumulative rainfall of previous five days. Due to its presence in the SCS-CN method (Ponce and Hawkins, 1996) for calculating antecedent basin conditions, this is index is widely used by hydrologists,
2. The logarithm of the discharge on the day before the flood event (*preQ*), as suggested by Brocca et al. (2009).
3. Soil moisture prior to the events from ERA5, representative of two different depths (i.e., 0–7 cm $SM1_{ERA}$ and 28–100 cm $SM3_{ERA}$).
4. Surface and root-zone soil moisture estimates obtained from GLEAM (which combines modeled and remotely sensed soil moisture from CCI) that are representative of 10 cm (SSM_{GLEAM}) and 90 cm (RZ_{GLEAM}) soil depths.
5. Modeled surface (SSM_{SAC}) and root zone (RZ_{SAC}) soil moisture estimates obtained from the continuous SAC-SMA hydrological model.
6. Pre-storm snow water equivalent (*SWE*) values obtained from ERA5.
7. Total water storage (*TWS*) at the beginning of the event (*preTWS*) calculated as residual of the water balance between time t and t-120 days: $preTWS(t) = \sum_{t-120}^{t}(P(t) - E(t) - R(t))$ where P was calculated from ERA5 precipitation, E is the evaporation derived from GLEAM and R is the total runoff (in mm) calculated from daily river discharge observations using basin areas. The accumulation over 120 days was selected to remove short-term scale changes of TWS and to isolate seasonal and inter-annual components of the TWS signal.

3.3. Basin classification

The selected basins cover many parts of Europe and are classified by their different land cover, climate, soil type, and hydrological signatures. As a result, systematically examining the influence of each individual factor on the coupling strength between *RC* and the different pre-storm condition proxies is challenging. To overcome this issue, we performed a basin classification using the *k-means* clustering algorithm (Lloyd, 1982).

This algorithm is among the oldest and most classical unsupervised learning algorithms used to partition datasets. It aims at portioning observations into K clusters defined by centroids, where K is chosen a priori. The algorithm has been applied in many fields due to its intuitive basis, high efficiency, and easy implementation (Chong, 2021). The partitioning is based on iteratively finding clusters (i.e., groups of basins) that minimize the sum of squared distance between the points of the cluster (within-cluster sum of square WCSS) and its centroid, and simultaneously maximize the distance between cluster centroids. As unsupervised learning, the algorithm detects patterns in the dataset using predefined distances such as Euclidian and exploits them.

In order to find an optimal number of clusters, we used the concept of Silhouette score (Rousseeuw, 1987). In the method of (Rousseeuw, 1987), each cluster is represented by a so-called silhouette (see Figure SI 8 in the supplement) which shows tightness and separation of each cluster for different number of clusters. The silhouette score is a measure of how similar an object is to its own cluster (cohesion) compared to other clusters (separation) (see supplementary material Section Supplementary Information 1.3 for further details on the method).

3.4. Regression analysis

The main objective of this section is to understand to what extent the different pre-strom proxies are able to explain the stormflow volume variability on top of precipitation. This was done by using Multi-Linear Regression (MLR) and Random Forest Regression (RFR). As predictors of stormflow volumes we selected, in addition to precipitation, the most highly correlated proxies with the *RC* (based on the correlation analysis in Fig. 5) as well as commonly used pre-storm proxies. These selected predictors are: P, RZ_{GLEAM}, *preQ*, *API*, *SWE* and SSM_{GLEAM} (the latter was used only for RFR given its potential collinearity with root zone observations).

For each basin we randomly selected 66% of events in calibration and the rest for validation. All presented results below are based solely on this validation period. To test the prediction capability of the different pre-storm proxies we carried out two different experiments: (1) we used only precipitation and antecedent precipitation index to predict stormflow volumes, and, (2) we used precipitation in addition to the pre-storm proxies mentioned above. RFR was also used to understand the feature importance of the different predictors.

Note that we are not so much interested in ML-based estimation of the stormflow volume in this manuscript, rather we leverage ML-based tools to rank the importance of different pre-storm proxies on top of precipitation.

3.4.1. Multi-linear regression

Multi-Linear Regression (MLR) is a statistical technique that employs several explanatory variables and one dependent variable, which in the present study is stormflow volume. In the MLR model, the dependent variable y is assumed to be a function of k independent variables x_k. The general form of the equation is computed as follows:

$$y_i = b_0 + b_1 x_1 + \ldots + b_k x_k + e \quad (1)$$

where b_0 and b_i are fitting constants; x_i is the *i-th* observation of each of the explanatory variables, y is the prediction of stormflow volume, and e is a random error term representing the remaining effects of variables on y, which are not covered by the model (residuals). The least squares criterion for the minimum sum of squares of error terms is usually applied to determine the fitting constants. We applied this approach here via the scikit-learn python package (Pedregosa et al., 2011). The main limitation of the MLR is that it requires the predictors to be mutually independent.

3.4.2. Random forest regression and feature importance

Random Forest Regression (RFR) modeling is an ensemble machine learning method for regression that operates by constructing a multitude of decision trees (Breiman, 2001). RFR modeling is appropriate for modeling the nonlinear effect of variables. RFR consists in building a forest of uncorrelated trees. Each individual tree is grown using a randomized subset of predictor variables to the largest extent possible without pruning and are aggregated via averaging. Since the individual trees cannot be examined separately, RFR does not calculate regression coefficients or confidence intervals (Cutler et al., 2007). Nevertheless, it allows for the computation of variable importance measures that can be compared to other regression techniques (Grömping, 2009). RFR can handle complex interactions among variables, and is not affected by multi-collinearity (Breiman, 2001). It can assess the effects of all explanatory variables simultaneously, and automatically ranks the importance of these variables in descending order (Rodriguez-Galiano et al., 2012). However, the main limitation of RFR is its inability to extrapolate values beyond the range of the training dataset, which makes it inappropriate for capturing hydrological extremes. For a detailed description of the mathematical formulation for the RFR model, the reader is referred to Breiman (2001), Liaw and Wiener (2002).

In this study, the open source scikit-learn RandomForestRegressor function was used https://scikitlearn.org/stable/modules/generated/sklearn.ensemble.RandomForestRegressor.html

To run the RFR model, it was necessary to first define a priori different RFR parameters (i.e., hypermaparameters). In the case of a random forest, hyperparameters include the number of decision trees in the forest and the number of features considered by each tree when splitting a node. These parameters control the way each tree is split during training. The best hyperparameters are usually impossible to determine in advance, so a trial and error procedure is necessary, which is based on a random search across a wide range of values for each hyperparameters. These parameters are in the case of the scikit-learn RandomForestRegressor the following ones:

- number of decision trees in the forest ($n_{estimators}$)
- max number of features considered for splitting a node ($max_{features}$)
- max number of levels in each decision tree (max_{depth})
- minimum number of data points placed in a node before the node is split ($min_{samplessplit}$)
- min number of data points allowed in a leaf node ($min_{samplesleaf}$)
- method for sampling data points (bootstrap) (with or without replacement)

Normally, the most important settings are the number of trees in the forest ($n_{estimators}$) and the number of features considered for splitting at each leaf node ($max_{features}$). To determine the above mentioned parameters we ran a grid search function using the GridSearchCV function of the same scikit-learn package (https://scikit-learn.org/stable/modules/generated/sklearn.model_selection.GridSearchCV.html) by letting the $n_{estimators}$ varying between 1000 and 5000 with steps of 100 and the number of features to vary between 1 and 10 with steps of 1. The logic to start from 1000 for the $n_{estimators}$ is because (Rodriguez-Galiano et al., 2014) demonstrated that the error was minimum and stable when considering at least 1000 trees, while, for the number of features the values were selected based on the recommendation of Breiman (2001) who suggested using m - where m equals the number of predictors (six in this case) divided by 3. The optimal number of these two parameters was then found based on the minimum mean squared error obtained in the validation sets of each basin. On top of regression analysis RFR allows one to estimate the variable importance of predictors in the explanatory model. This is done by the mean and standard deviation of accumulation of the impurity decrease within each tree calculated via the Gini index (which measures the quality of a split for each variable in a tree, that is the node impurity or lack of information of the explanatory factors, see again Breiman (see again 2001, for further details).

4. Results and discussion

4.1. Runoff coefficient variability, flood seasonality and relation between precipitation, event peak discharge and stormflow volume

The event extraction resulted in a distribution of *RC*s that shows smaller values and much larger variability (quantified using the coefficient of variation, *CV = mean/standard deviation*) over the Mediterranean area and Eastern UK while larger *RC*s less variable are seen over central Europe and Northern and Western Iberia Peninsula (see Fig. 2). This is consistent with results in Merz and Blöschl (2009) in Austria and Norbiato et al. (2009) in Northern Italy, who reported that mean *RCs* are strongly correlated to indicators representing climate such as mean annual precipitation.

For the majority of the basins, the extracted flood events occurred in wintertime, especially in central Europe, while 30%–50% of events in southern Europe occurred during the fall. Percentages below 30%–40% are observed elsewhere during the spring (Fig. 3). A high frequency of flood events during the summer is seen only over the Alps.

To identify the strength of the relationship between flood and precipitation, we plotted in Fig. 4 the box plots of the intra-basin Spearman correlation obtained between event-based precipitation volumes and: (i) event-based peak discharge of all extracted flood events (*cor-peak*), (ii) event flow maximum annual peak discharge (*cor-peak-max*), (iii) event-based stormflow volumes (*cor-vol*), and (iv) maximum annual stormflow volume (*cor-vol-max*). From the figure it can be seen that peak discharge is in general less related to precipitation with respect to stormflow volumes particularly for large flood events — a result in general expected (see Berghuijs et al., 2019; Stein et al., 2021; Do et al., 2020). On the contrary, flood volumes seems well correlated with the precipitation and not particularly impacted by the relative magnitudes of the events.

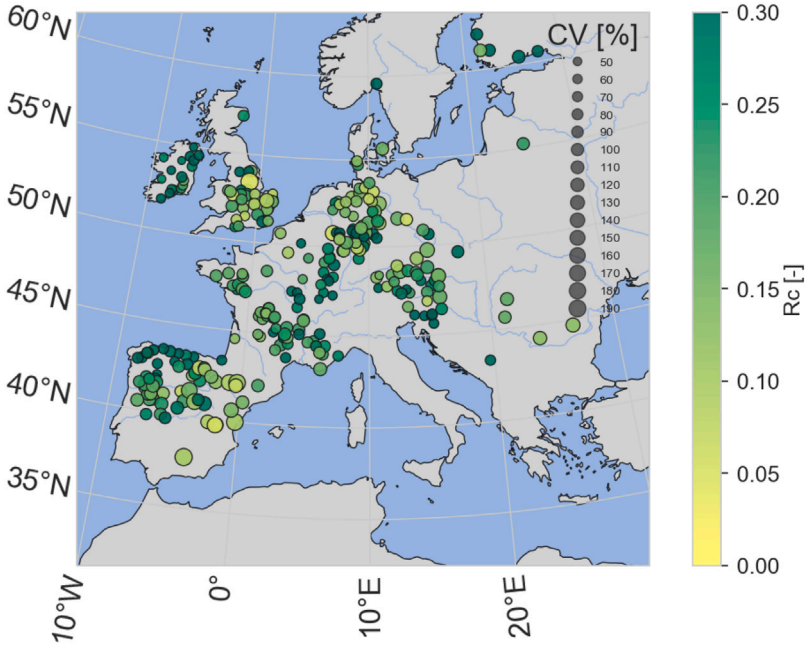

Fig. 2. Spatial distribution of the median RC(*RC*). The size of the dot is proportional to the coefficient of variation (CV) of *RC* across the selected flood events.

Note, however, that box plots in Fig. 4 are highly scattered suggesting other potential mechanisms controlling the response in terms of both volume and discharge beyond precipitation like for instance antecedent conditions (see Section 4.4). This is particularly true for peak discharge being it dependent also on residence times. *RC* modulates the relationship between precipitation and both peak discharge and stormflow volumes as shown in Figure SI 5 of the supplement, where the Spearman correlation coefficient between precipitation and the two variables is plotted for five equi-populated bins of *RC*. As expected, correlations tend to increase for events characterized by larger *RC* (with a tendency to decrease for *RC*s larger than one when considering stormflow volume). This emphasizes the enhanced role of low *RC* in modulating the response of the basins to precipitation. Additional potential elements inducing this relatively large spread are the quality and the spatial resolution of the data used in this analysis. Nonetheless the analysis in terms of peak discharge remains difficult at the daily time scale being river discharge not conservative unlike volumes.

4.1.1. Overall relation between runoff coefficients and pre-storm condition proxies

Fig. 5 shows box plots of the Spearman correlation coefficient computed between the *RC* of recorded flood events and different pre-storm condition proxies for each of the 284 basins. Although the correlation coefficients have large variability, a consistent increase in the correlation for pre-storm proxies related to deeper (darker colors) soil storages emerges (e.g., RZ_{GLEAM}, $SM3_{ERA}$ and $preTWS$ show higher median correlations). Note that being representative of root zone RZ_{GLEAM}, $SM3_{ERA}$ are essentially more mutually correlated with respect to the other proxies (see Figure SI 6 in the supplement) while $preTWS$ also depends on snow and other storages in the basin so its mutual correlation is lower than between the previous two (see also Section 4.3). Relatively higher correlations with *RC* are also found for pre-storm river discharge and pre-storm snow water equivalent. Shallow storages like SSM_{GLEAM}, $SM1_{ERA}$ show worse results while for both API and hydrological model states (SSM_{SAC} and RZ_{SAC}) correlations are weaker. The poor performance of the SAC states model can be attributed to the overall relatively low performance of the model (median *KGE* below 0.6, see Figure SI 7 in the supplementary material) while the very low correlations of *API* are not expected a priori. Note that we cannot extrapolate the result of SAC-SMA to hydrological models in general as we only considered one model and one calibration technique; however, it should also be mentioned that, as opposed to the other proxies, the SAC model is directly calibrated against the river discharge observations. Although we used state-of-the-art calibration techniques, such calibration entails some levels of subjectivity, so that no general conclusions should be drawn for this particular result.

The correlations in Fig. 5 are in any case generally low. This is not surprising since we examined a wide spectrum of basins characterized by different topography, climate, land cover and hydrological behaviors (see Section 2.1 and Fig. 1) and because we did not separate between seasons (and therefore main flood generation mechanisms). On top of that, uncertainties in this analysis arise from the quality of precipitation and river discharge datasets, as well as the use of daily data — that can limit the identification of the exact timing of the flood peaks and thus the correct identification of precipitation and pre-storm proxies. Nonetheless, inherent uncertainty of the used proxies might play also an important role. A final remark is related to the flood occurrence which is concentrated mostly during the winter season, when the storage variability of the basins is expected to be lower than in the other seasons (see Section 4.3).

4.2. Basin classification

Figs. 5 helps us understand the overall relation between pre-storm proxies with *RC*. However, it also reveals a large spread and modest correlations that may hide the role of the basin in influencing the response to precipitation. Therefore, we grouped basins with similar attributes to clarify the coupling strength between pre-storm conditions and *RC* by categorizing different types of basins using an unsupervised clustering algorithm (see Section 3.3) based on land cover (*CN*), climate (*AI*), topography (*elev* and *tc*), and hydrological signature (*bfi*, *fl* and *vi*) (see Fig. 1). The partitioning was performed by *k-means* by choosing the Euclidean distance as a metric with a number of clusters found equal to 5 following the Silhouette criterion (see Figure SI 8 in the supplement and Section 3.3). Note that, relative to the work of Kuentz et al. (2017), our experiment is much simpler — as we only used static features to define the classes, and we performed the classification on only 284 basins.

Fig. 6 shows the distribution of the different basins descriptors as a function of the class while Fig. 7 their geographical distribution. Based

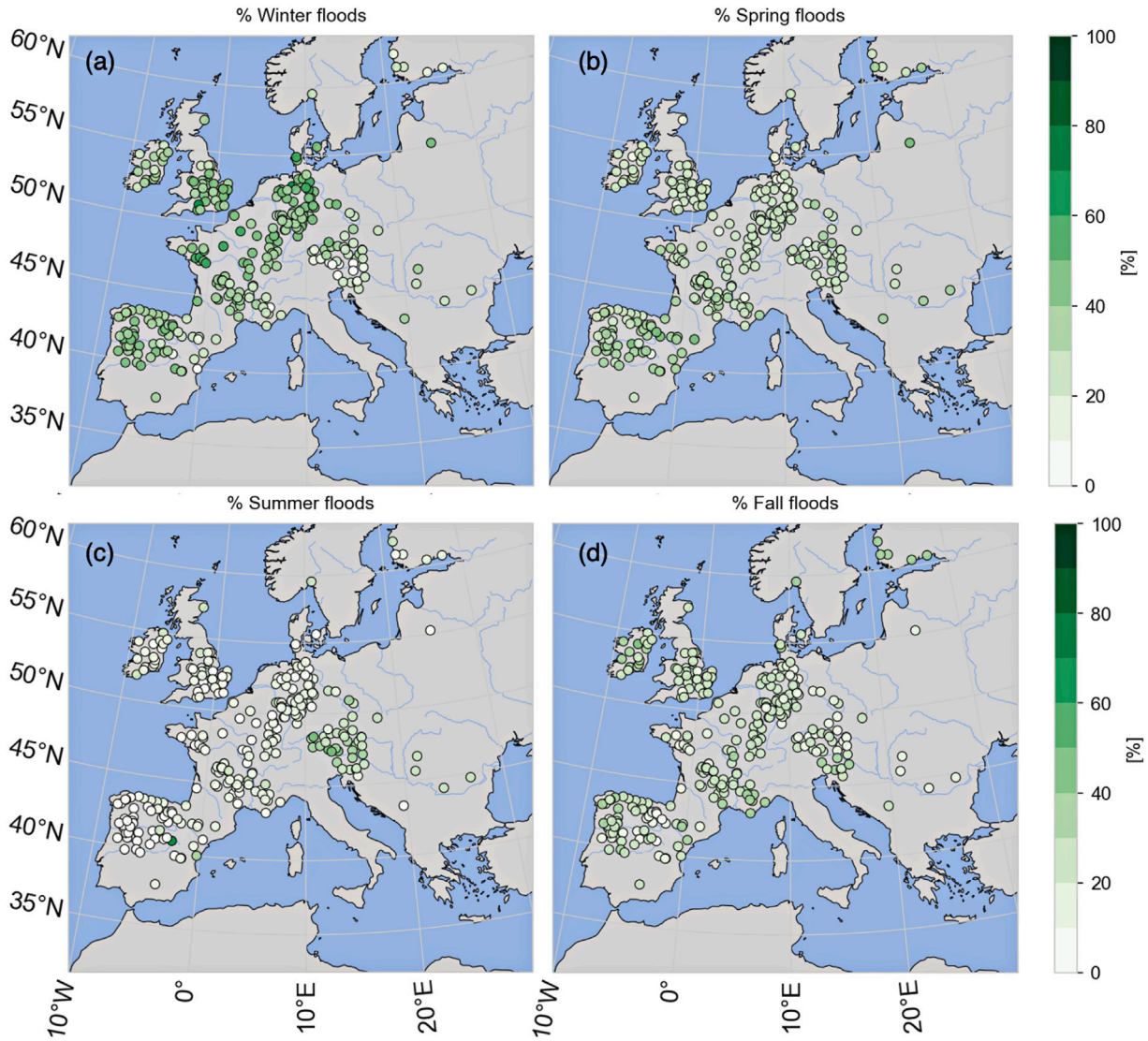

Fig. 3. Percentage of flood events occurred in the winter (December–January–February) (a), spring (March–April–May) (b), summer (June–July–August) (c) and fall (September–October–November) during the period 1980–2016.

on the distribution of the predictors the characteristics of the classes are summarized below:

1. Class 1: typically mountainous basins characterized by complex topography, high elevations and energy limited climate. Low permeability, low flashiness, and high baseflow index. These are snow dominated basins belonging to the alpine range, Pyrenees, and other mountainous chains of the Iberia Peninsula.
2. Class 2: hilly to mountainous basins with relatively warm climate (mainly water limited). They are characterized by low *bfi*, higher variability, and flashiness. These basins are almost exclusively concentrated in the Mediterranean area.
3. Class 3: flat cold basins, with high *bfi* and small variability and flashiness typical of northern latitude flat basins where groundwater and infiltration seems to dominate. These basins are located mainly over flat lands around the Baltic and Northern Sea.
4. Class 4: flat basins in transition between the energy limited and water limited regions (likely subjected to annual alternation between these two regimes) characterized by low *bfi*, medium hydrological variability (i.e., *vi*) (although less than Class 2) and high flashiness (the contribution of groundwater is expected to be lower than Class 3). What distinguishes Class 3 from Class 4 is the contrasting hydrological behavior and the warmer climate for the seconds. Class 4 basins are much more responsive than Class 3 basins thanks to the larger fraction of impervious surfaces suggested by *CN* (Fig. 6).
5. Class 5: hilly and cold basins with a large fraction of pervious surfaces with medium flashiness and medium *bfi*. These basins do not show a clear geographical pattern (see below).

It should be noted that the aridity index (*AI*) plays an important role in the distinction among the classes, as also found by Kuentz et al. (2017). In fact, *AI* sets sharp separation between classes 1, 3, 4 and 5 (placed across energy limited regions) with Class 2 (e.g., the Mediterranean area). For the energy limited regions the distinction between Class 3 from Class 4 is mainly based on the basin response, with the first being characterized by low flashiness and high baseflow, and the second by flashy behavior and low baseflow, where groundwater contribution is expected to be lower. Finally, Class 5 is the most uncertain one providing average values in terms of hydrological response in relation to Class 3 and Class 4. However, it is interesting to note that basins of Class 5 reflect the climate organization of temperate humid with cool summer (i.e., Cfc, according to Köppen–Geiger) as also seen in Beck et al. (2018). Basins belonging to Class 5 are different from the ones in Class 3 and Class 4 from the fact that basins belonging

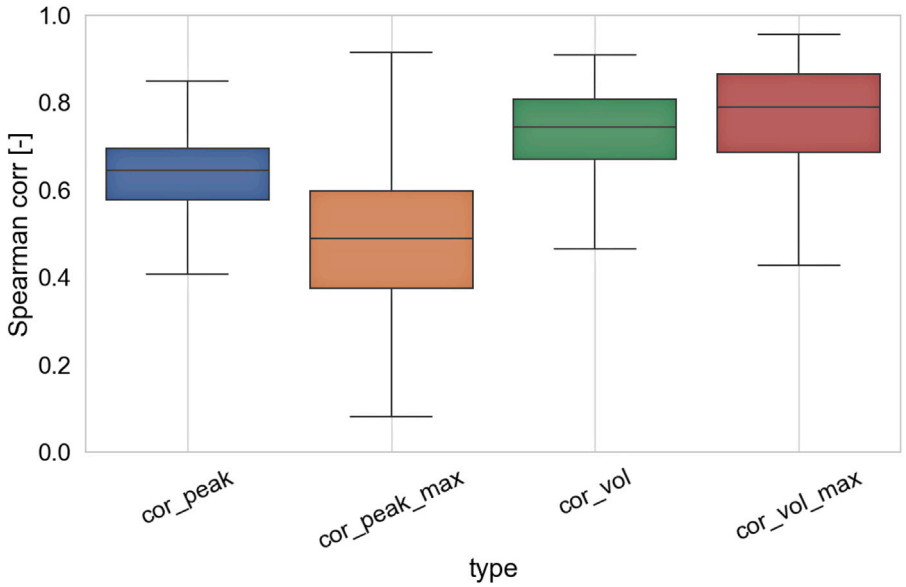

Fig. 4. Box plots of the intra-basin Spearman correlation (across all basins) obtained between event-based precipitation volumes and (i) stormflow peak discharge of all extracted flood events (*cor-peak*), (ii) stormflow maximum annual peak discharge (*cor-peak-max*), (iii) stormflow volumes (*cor-vol*), and, (iv) maximum annual stormflow volume (cor-vol-max). In the box plots the different lines refer to the median, the interquartile, the minimum and maximum.

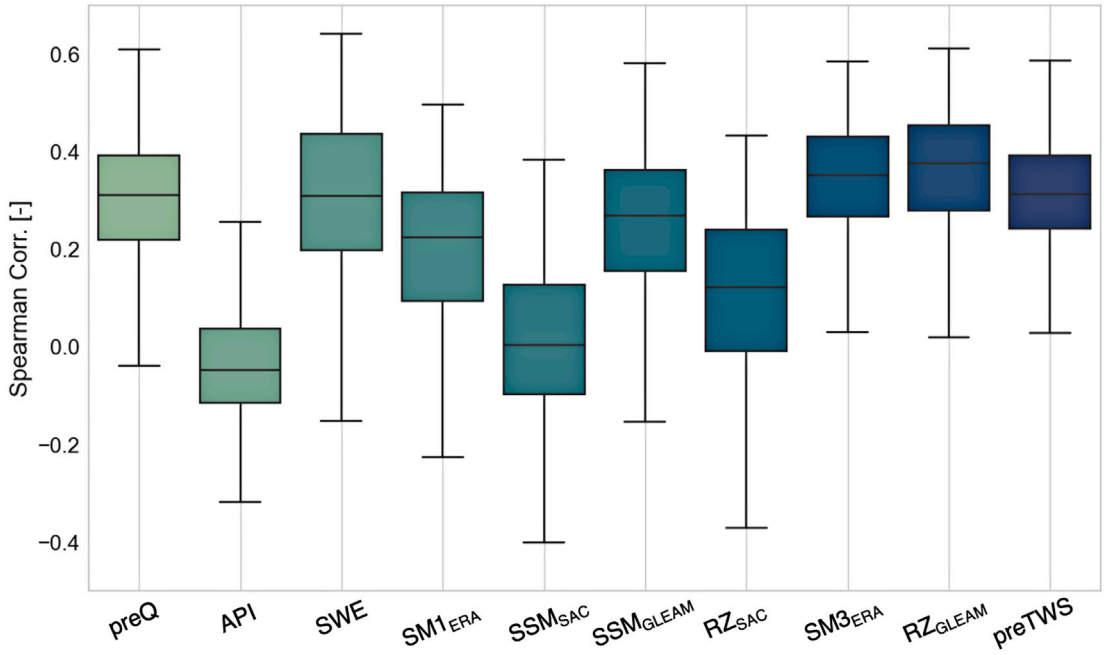

Fig. 5. Spearman correlation coefficient between *RC*s and basin pre-storm condition proxies: pre-storm river discharge (*preQ*), Antecedent Precipitation Index (API), Antecedent Snow Water Equivalent (SWE), the surface (SSM) and root zone (RZ) soil moisture simulated by Sacramento Hydrological model (SAC), GLEAM and ERA5 ($SM1_{ERA}$ and $SM3_{ERA}$), and the calculated pre-storm total water storage anomalies (*preTWS*) and pre-strom snow water equivalent (*SWE*). Darker color reflects deeper storage representations except for *preQ*, *API* and *SWE*.

to it are placed on hilly terrains (versus flat) and have a much higher percentage of pervious surfaces as indexed by their *CN* distribution. For the energy limited regions the distinction between Class 3 from Class 4 is mainly based on the basin response, with the first being characterized by low flashiness and high baseflow, and the second by flashy behavior and low baseflow, where groundwater contribution is expected to be lower. Finally, Class 5 is the most uncertain one providing average values in terms of hydrological response in relation to Class 3 and Class 4. However, it is interesting to note that basins of Class 5 reflect the climate organization of temperate humid with cool summer (i.e., Cfc, according to Köppen–Geiger) as also seen in Beck et al. (2018). Basins belonging to Class 5, differently from the ones in Class 3 and Class 4, are placed on hilly terrains (versus flat) and have a higher percentage of pervious surfaces, as indexed by their *CN* distribution.

To understand any possible relation between *RC* distribution and the specific class, we plotted in Fig. 8 the different distribution of runoff coefficients corresponding to each class. It can be seen that the largest *RC* variability is observed for Class 2, which also shows the largest fraction of events with small *RC* value. This is likely due to the warm climate and normally dry conditions, that let precipitation infiltrate more easily. Conversely, cold basins as those in mountainous areas and northern regions (Class 1 and Class 5) show a large fraction of high *RC*s,

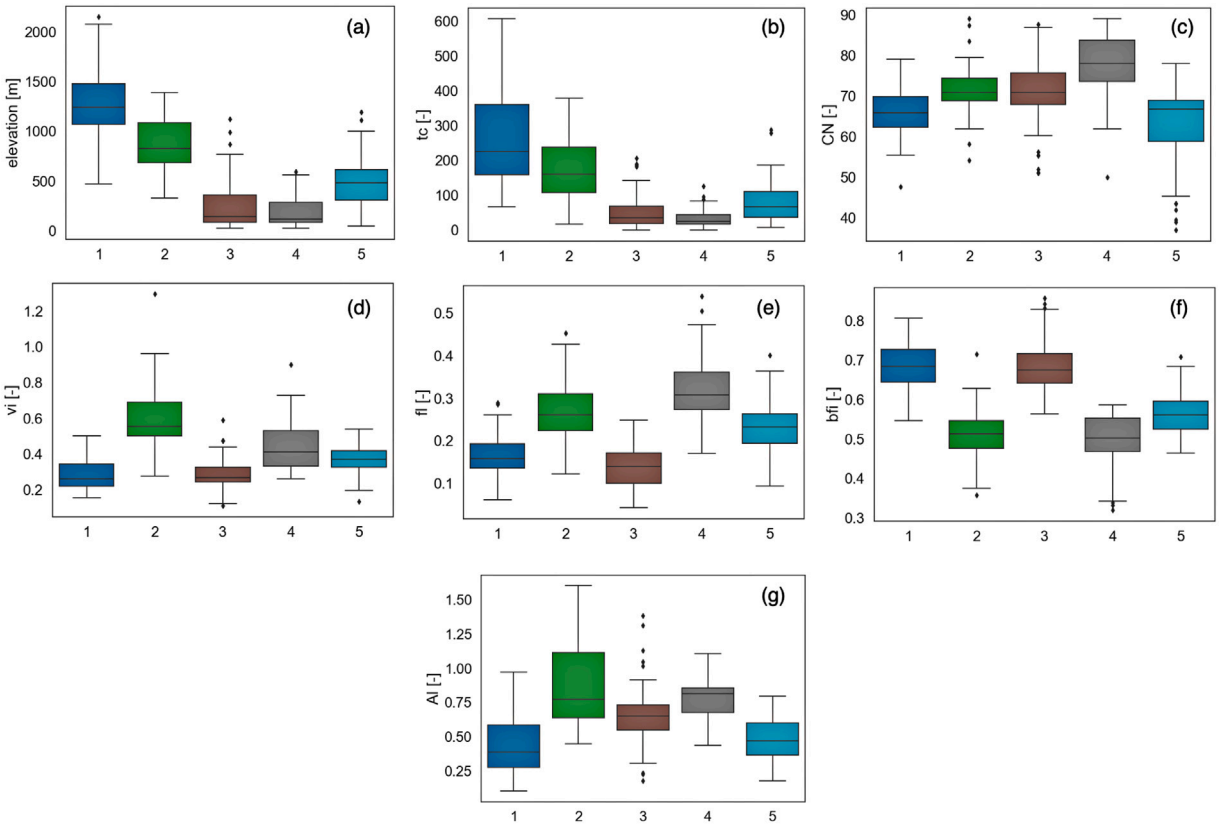

Fig. 6. Distribution of the different basin descriptors (land cover and soil as indexed by the curve number – *CN*, aridity index – *AI*, topography – elevation, *elev*, and topographic complexity, *tc*), hydrological signature – baseflow index *bfi*, flashiness, *fl*, and hydrological variability, *vi*), as a function of the class.

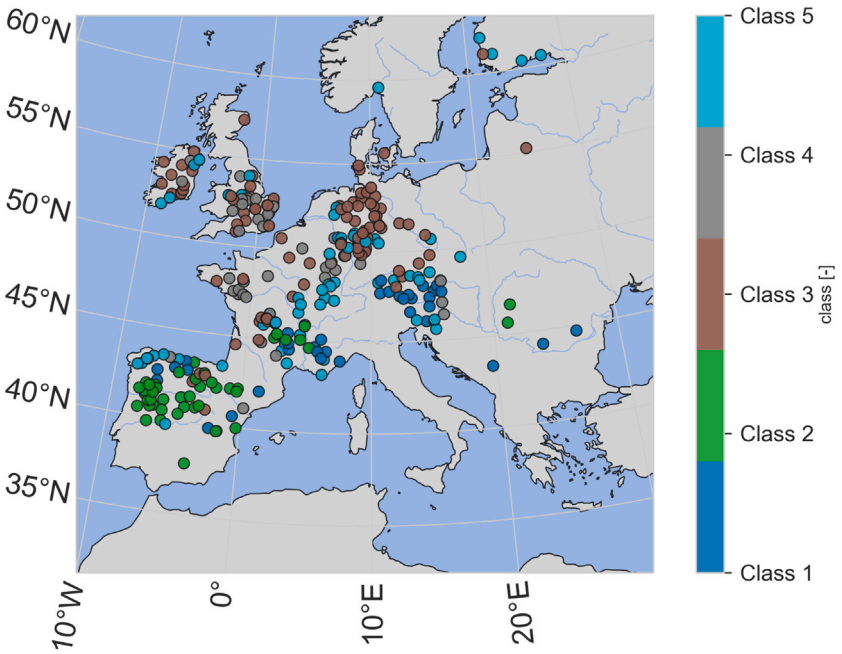

Fig. 7. Basin classification obtained by the *k-means* clustering algorithm.

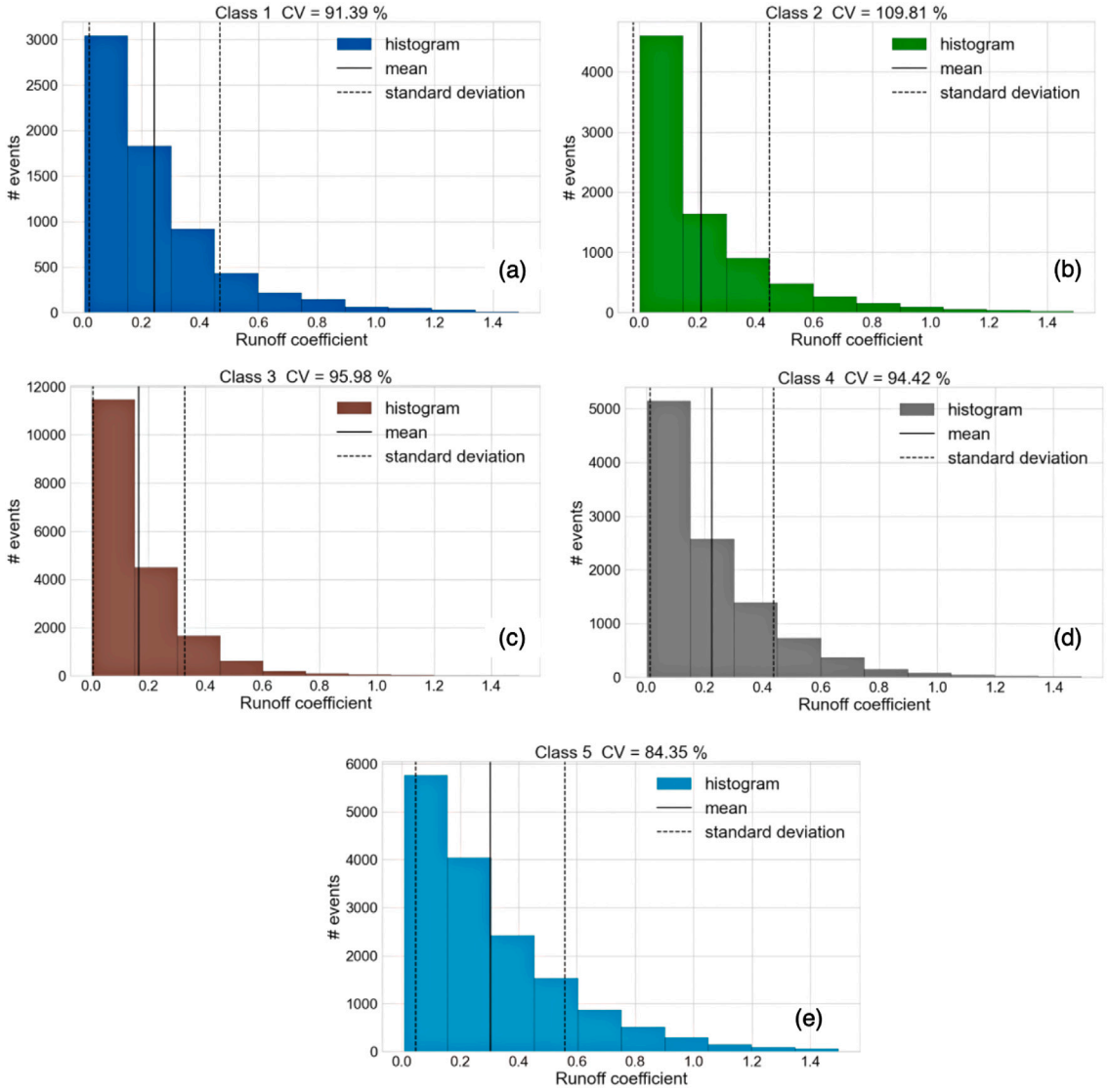

Fig. 8. Runoff coefficient distribution within the five identified classes. CV refers to the Coefficient of variation. (a) Class 1, (b) Class 2, (c) Class 3, (d) Class 4, (e) Class 5.

potentially due to snowmelt process and saturated soils. Finally Class 3 and Class 4 (flat basins with contrasting hydrological regimes) show some differences in the distributions, with Class 4 showing a larger fraction of high *RC*s probably favored by lower permeability of the surfaces (see *CN* in Fig. 6c), and Class 3 characterized by very flat terrain and larger infiltration capacity (as demonstrated by the large *bfi* in Fig. 6d).

Fig. 8 can be considered a sort of cross validation of the clustering, as no information on *RC* has been used to identify the clusters. Furthermore, it shows consistent results with literature by demonstrating the link between *RC* and basin attributes and therefore, potentially, between precipitation and related flood magnitudes (Komma et al., 2007; Berghuijs et al., 2016; Breiman, 2001; Slater and Villarini, 2016; Breinl et al., 2021). The interplay of these factors determines the specific behavior of the basins in response to precipitation. For example, over cold and wet basins event *RC*s tend to be higher due more constant saturated soil conditions and snowmelt contribution, thus strengthening the relation between flood and precipitation frequencies (Borga et al., 2007). Across warmer basins, where also other factors might play a role like infiltration-excess (Yair and Klein, 1973), soil moisture is more seasonally variable than in more humid basins, and weaker relationships between precipitation and floods are expected (Sivapalan et al., 2005; Merz and Blöschl, 2009).

4.3. Relation between runoff coefficient and pre-storm proxies as a function of type of basin, season and climate

Fig. 9 displays the intra-basin Spearman correlation coefficient between *RC* and different pre-storm proxies for the five classes. The figure reflects in general the results obtained in Section 4.1.1, with relatively low correlations for *API* and SAC model states, medium low ones for surface soil moisture proxies, and higher for deep water storages, pre-storm river discharge and snow water equivalent. The last three, in particular, show different behaviors depending on the class.

In Class 1 (typically mountainous basins) pre-strom *SWE* shows the highest correlation, suggesting that *RC*s here are mainly driven by snowmelt. The latter is followed by pre-strom deep water storage in particular by RZ_{GLEAM} and *preTWS*. All the other proxies seem to have a poor relation with *RC*.

Class 2, which contains basins located in warmer climates, shows a larger importance of deep pre-strom proxies and pre-storm river discharge, with medium-to-low correlations for surface soil moisture, although higher than in Class 1 (see the $SM1_{ERA}$ in particular). This is consistent with earlier results from Tramblay et al. (2010), Brocca et al. (2009), who found a strong relation between soil moisture and *RC* over the Mediterranean area. In general in Class 1 and Class 2, that are the classes characterized by more complex topography and higher

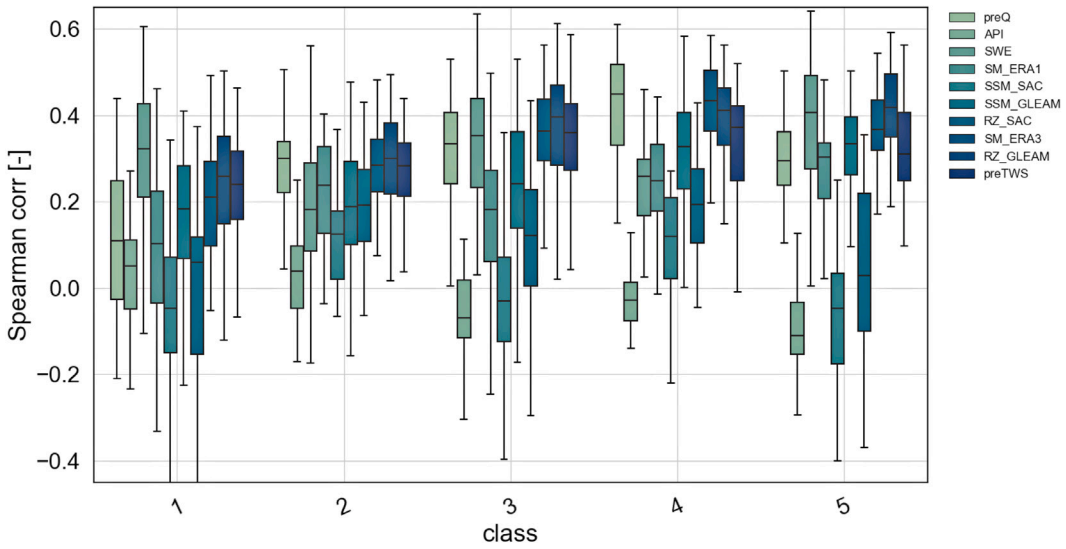

Fig. 9. Same as Fig. 5, organized by class.

elevations (see Fig. 6), the overall agreement of pre-storm proxies with *RC* is lower than in the other classes. This is likely due to the effect of the slopes and other factors controlling *RC* variability (Tarasova et al., 2018).

Class 3 contains flat cold basins with high *bfi*. Here, the situation seems to mirror Class 2, but with one important exception related to the larger importance of pre-storm *SWE*. Also here, deep soil storage pre-strom proxies are generally characterized by higher correlations with respect to the other proxies (more than in Class 1 and Class 2). Here, the root zone SAC model state (i.e., RZ_{SAC}) shows higher correlations with respect to the other classes, likely due to the better performance of the model across higher latitudes (see Figure SI 7 in the supplement).

For Class 4, which contains basins generally warmer than Class 3 and characterized by an opposite hydrological behavior (high flashiness and variability and much lower *bfi* similar to the one in Class 2), pre-strom river discharge shows the highest correlation with *RC*, depicting its relatively high importance in flood forecasting. In these basins, snowmelt seems much less important than in Class 3 (as expected from the *AI* distribution). At the same time, pre-storm soil storages are also better correlated with *RC* and show an interesting inversion of the scores of the RZ_{GLEAM} and $SM3_{ERA}$, with the latter better than RZ_{GLEAM} in Class 4 with respect to Class 2, and vice versa. The reasons for this are not clear but reflect patterns of assimilation results of De Santis et al. (2021), who found, over southern European latitudes, better performance of satellite surface soil moisture observations in improving river discharge simulations than in northern latitudes. Note that however that this would require further analyses to be demonstrated. RZ_{SAC} reflects the results of Class 3, likely due to the better performance of the SAC model.

Finally, for Class 5, containing cold basins with pervious surfaces (mostly natural basins based on the *CN* distribution), the distributions of correlations among the proxies is very similar to Class 3, with a stronger correlation of pre-storm snow water equivalent with *RC* for Class 5 (higher with respect to Class 3).

Fig. 10 show the Spearman correlation coefficient obtained by pre-strom proxies and *RC* for all the events belonging to a certain class as a function of the season. To take into account sampling uncertainty, we used bootstrap with 500 replicates by randomly sampling 70% of the events for each replicate (error bars on the histogram bars).

It can be seen that Class 1 shows a general poor correlation between *RC* and pre-storm proxies during the winter season, when the basins are normally wet and the cold temperature makes the *RC*s less variables due to the lower atmospheric demand. As expected, during spring and summer these correlations increase significantly, especially for pre-strom SWE and *preTWS* (which likely contains the snow signal in it). During summer and fall, correlations remain moderate, with an increase in the correlations of deep soil water storage during fall and of surface soil moisture during summer.

Class 2 shows similar correlations between winter and spring, and a drop during summer. The lower agreement between *RC* and pre-storm proxies during the summer can be explained by the higher chance of convective precipitation during this period, which increases the chance of infiltration-excess runoff generation process. This is in line with the results of Castillo et al. (2003), who found that in hot semiarid and arid environments with drier soils, the role of antecedent soil moisture is generally less important. They attributed this to the controlling runoff mechanism of infiltration excess overland flow, as opposed to saturation excess (also confirmed by Zhang et al. (2011). Indeed, during fall, we observed again a marked increase in correlations for *preQ* and deep soil storages (a results generally observed for all classes).

For Classes 3, 4 and 5 the correlations of the proxies with *RC* during winter are relatively low, especially for soil water storage (with even no correlation for Class 5). These correlations tend to increase for pre-storm *SWE* during spring, especially for the coldest basins of Class 5. These results only partially confirm the results of Berghuijs et al. (2019), who found that floods in Europe are almost exclusively driven by soil moisture excess with minor impact of snowmelt and extreme rainfall. Conversely, our results suggests that during spring snowmelt can have an important contribution in runoff generation. During summer deep pre-storm soil moisture storage correlations increase for both Class 3 and Class 4, along with surface storages for Class 3 (which is characterized by a more flashy behavior). Note that during summer we observe higher correlations also for surface soil moisture proxies for Class 4, which look equally important to their respective root zone parts. This could be related to the higher flashiness of these basins with respect to the other classes, which would cause a larger impact of surface layers in determining the response to precipitation inputs. This is confirmed by the poorer correlation of the SAC root zone soil moisture with respect to its surface counterpart. In fact, the model tends to use shallower soil moisture states to simulate flashy runoff response. Finally, during fall, all classes show a marked increase in the correlation of *preQ* (probably proxy of groundwater contained in the basins during these periods) and deep soil storages. Here, the correlation between *RC* and pre-storm proxies is generally higher than during the other seasons, as precipitation tends to replenish soil moisture following summer evaporation, thus providing a rather direct link between soil

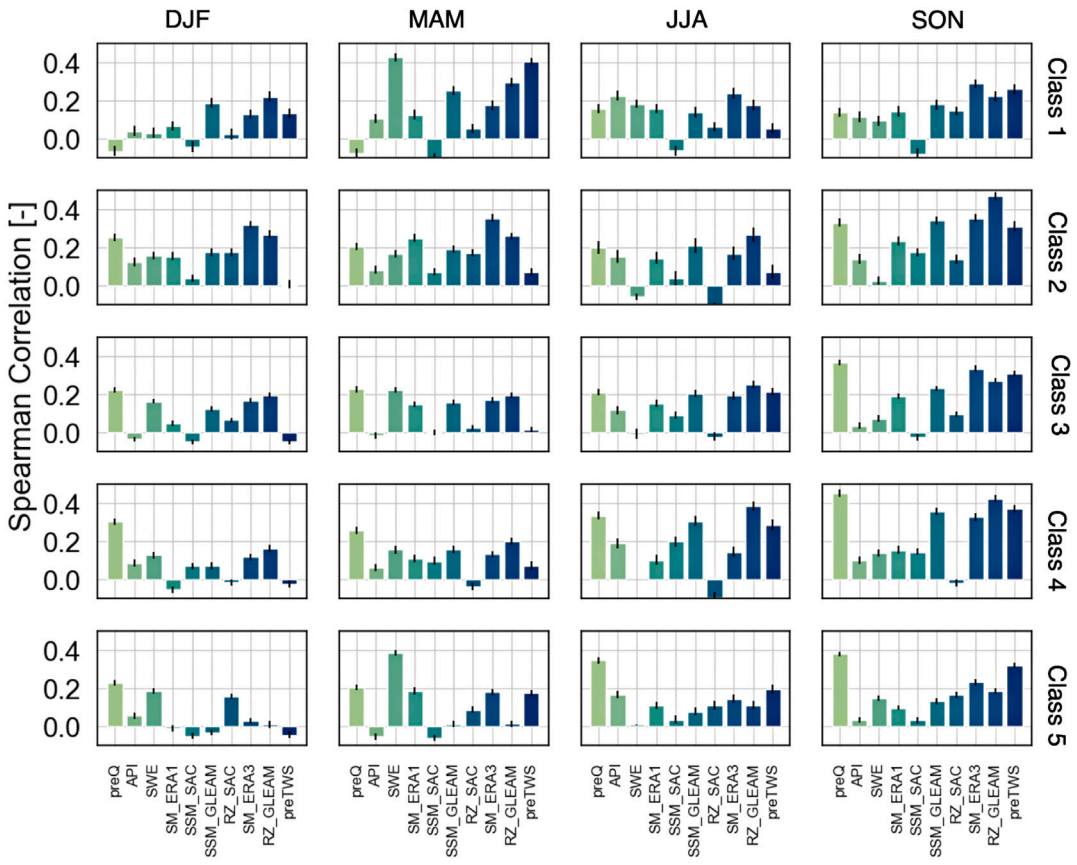

Fig. 10. As Fig. 8 but stratified for different seasons (DJF: December, January, February, MAM: March, April, June, SON: September, October, November). Each row refers to a class, namely Class 1 first line, Class 2 second line, Class 3 third line and Class 4 fourth line. Error bars refer to two standard deviations.

moisture and *RC*. These results reflect results of Berghuijs and Slater (2023) who found antecedent baseflow and groundwater important for shaping floods across north American rivers basins.

Fig. 11 shows the Spearman correlation coefficient between the pre-storm conditions proxies and *RC* within the different classes as a function of long-term precipitation anomalies as indexed by the Standardized Precipitation Index (SPI). To calculate the SPI we used the exponentiated Weibull distribution, as suggested by Pieper et al. (2020), and an accumulation period of 12 months (SPI12, McKee et al., 1993). Values of SPI12 are indexed commonly as: $SPI12 <= -1$: drier than normal, $-1 < SPI12 < 1$: normal and $SPI >= 1$: wetter than normal). In the figure, we note generally lower correlations (except for Class 2) during wet periods, as opposed to medium and dry periods, for deep soil water storage proxies, especially for soil water storage proxies and particularly for *preTWS*. This result is expected for classes located in energy limited environments because these basins, during wet periods ($SPI >= 1$), are generally subjected to constant saturated soil conditions and lower storage variability (and specifically for *TWS*). Conversely, for normal periods and periods drier than normal, the soil storage variability is expected to be higher because of stronger effect evaporation. This higher variability translates into a stronger coupling between *RC* and the different pre-storm soil storage proxies.

Unlike the other classes, in Class 2 the coupling between *RC* and pre-storm proxies for normal periods and periods wetter than normal remains high. For these basins, mostly located in a water limited-regime, the stronger influence of evaporative demands with respect to energy limited basins induces more frequent and intense cycles of wetting and drying also during normal and wetter than normal periods (with respect to drier than normal ones). This will likely increase the coupling between *RC* and soil storages and so the larger correlations. This is however not reflected in *preTWS* (which contains the total water contained in the basin, including snow, groundwater and soil water) as its longer memory and its close relation to the groundwater signal in these warm basins makes it less impacted by short term climate variability. This finding related to *preTWS* is true also for Classes 2, 3 and 4, while the snow influence on *preTWS* in Class 1 and Class 5 significantly reduces this drop in correlation. For Class 2 it is interesting to see how *preQ* changes its relative importance by moving from dry to wet periods because, in wet periods, it is more related to the water stored in the basin. In Class 1, pre-storm *SWE* increases its relation with *RC* during humid periods (more snowy as expected), while Class 5 seems basically not impacted by SPI.

For Classes 2, 3 and 4 surface soil moisture estimates (i.e., $SM1_{ERA}$ and SSM_{GLEAM}) seem to be more strongly coupled with *RC* in periods that are drier than normal, especially for Class 4 (flashier basins) where SSM_{GLEAM} reaches correlation equivalent to root zone soil moisture products.

4.4. Regression analysis

In this section, we applied regression techniques defined in Section 3.4 to understand to what extent the different pre-strom proxies are able to explain the stormflow volume variability on top of precipitation.

Fig. 12 shows the distribution of the coefficient of determination obtained across the five classes of basins for the two regression techniques in the two configurations with all predictors (RFR-F and MLR-F) and with only precipitation and *API* (RFR-B and MLR-B). It can be seen that in general both MLR-F and RFR-F provide better scores with respect to MLR-B and RFR-B (except for class 1 for RFR). This points to the importance of the pre-storm proxies in the generation of flood volumes for all classes. In particular, MLR outperforms RFR, likely due to the worse ability of the latter to extrapolate across magnitudes not present

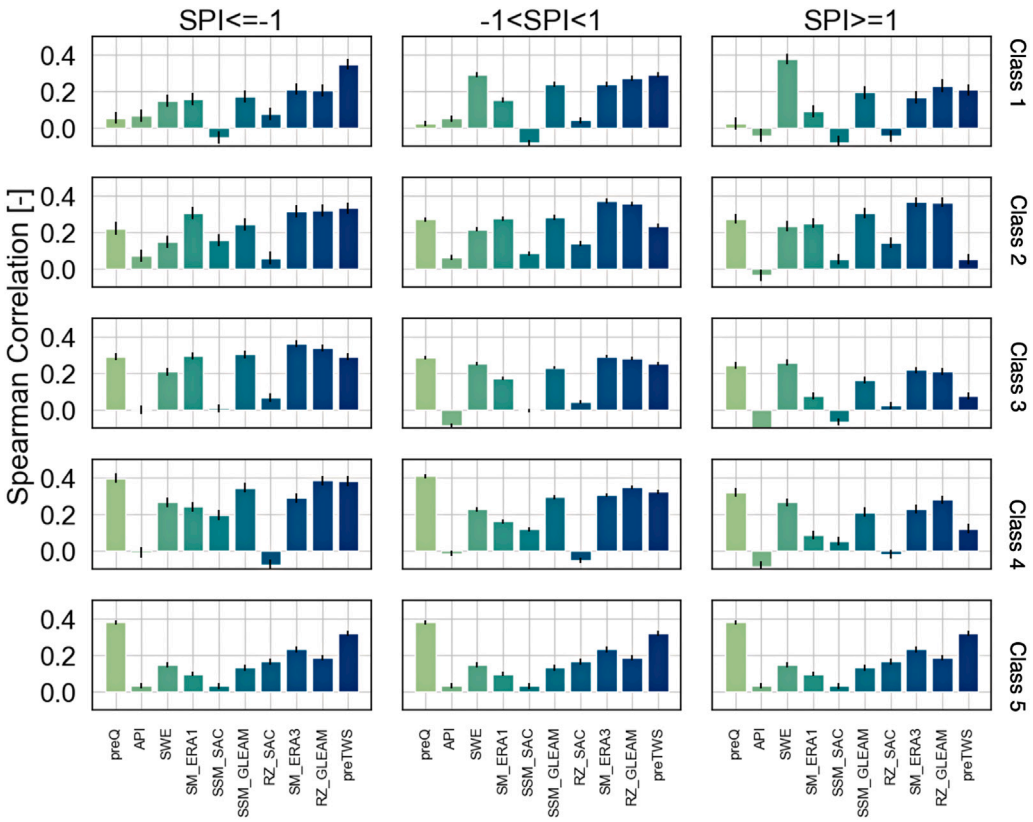

Fig. 11. As Fig. 11 but stratified per climate periods (i.e., drier than normal in the first column, normal in the second column and wetter than normal in the third column).

in the training dataset (despite the lower number of predictors used in MLR).

As RFR-F provides a way to calculate the importance of the different predictors, we displayed in Fig. 13 the rank of their importance obtained by comparing the mean of the feature importance obtained across the five classes. As expected, precipitation is the most important predictor while pre-storm *SWE* plays a key role (it ranks second among the six predictors) in Class 1, 3 and 5 which are characterized by relatively cold climates. In Class 2 and Class 4 river discharge seems to play also an important role, followed by root zone soil moisture in Class 2 and *SWE* in class 4. The importance of root zone soil moisture ranks third or second in many cases, indicating an overall high importance – as also suggested by Fig. 5. Finally, surface soil moisture and antecedent precipitation index seem to play a minor role in all classes. These results corroborate the correlation analysis done in Fig. 5 and can thus be considered further proofs of the behavior of the basins we described in the previous sections.

Given that these results refer to all periods and all events, it is likely that the relative rank can change based on seasons/climatic periods, as shown in Section 4.3. Furthermore, despite the pattern of improvements obtained by RFR reflects that of MLR, and thus the calculation of the feature importance can be considered reliable, the performance of the RFR-F experiments are not excellent. This makes the derived ranks inherently uncertain. In this respect, it is important to note that the regression experiments carried out here do not have the goal to demonstrate the ability these techniques to forecast flood volumes but only to show the relative contribution of pre-storm proxies in the generation of runoff. It is likely that more complex regression techniques or well calibrated (directly on flood events) hydrological models can achieve performances far better than the ones obtained here.

4.5. Limitations of the study

Our results focus on European basins only, and are limited by the size of the examined basins and by the resolution of the used datasets. We call for further large-scale experiments in other parts of the world and for further investigation at finer scales, for example with better, more explicit and more controlled consideration of local factors, such as basin features, hydrological regimes, and anthropogenic influences. Indeed, the large-scale relationships found in this multi-basin study may not hold for individual basins, as various underlying physical processes can impact basin hydrological behavior, such as specific geological and climatological conditions, anthropogenic influences, complex hydrological regime, and more local basin processes. In this respect, our basin classification could be sub-optimal especially across northern latitudes as also highlighted by Kuentz et al. (2017). Furthermore, at the scale of the European continent, large-scale gridded data as those used in this study, provide only a rough approximation of the occurring precipitation (Hofstra et al., 2009), as the grid cells are averaged over considerable spatial heterogeneity. The latter, in particular, introduces additional conditional bias issues determining potential underestimation of extreme precipitation. As a result, individual rain storms recorded in the data set will not always reflect local basin conditions. For example, true maxima may be obscured, challenging an accurate attribution of flood drivers on an event basis. This also holds for the large-scale soil moisture and evaporation products used in this study, which not always accurately represent the event-scale basin conditions. Finally, the basin size considered in this study and the daily granularity of the analysis can hide the small-scale temporal variations of hydrological conditions. In this respect, our analysis could be strengthened by focusing on a selected sample of basins with higher temporal- and spatial-resolution data. Nevertheless, the fact that we found a clear statistical large-scale signal of dominant correlations between different pre-storm proxies and *RC*s for different datasets from different data sources and for a variety of basins with different local

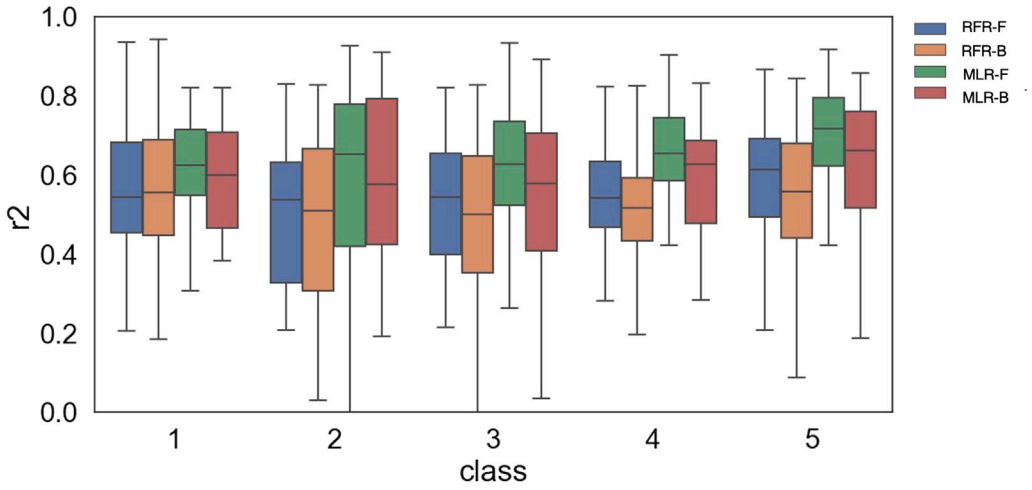

Fig. 12. Coefficient of determination distribution (r2) across the different classes of basins for the regression techniques using random forest and multi-linear regression using all predictors (MLR-F and RFR-F) and with only precipitation and *API* (MLR-B and RFR-B).

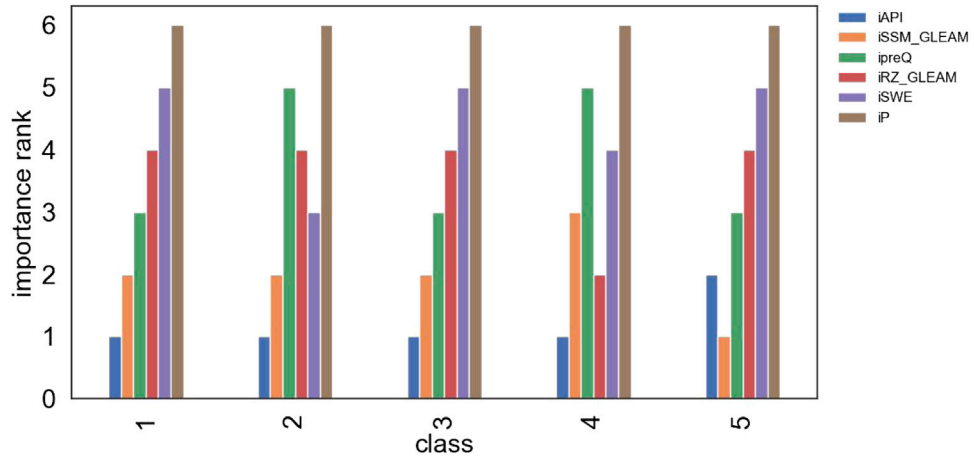

Fig. 13. Rank of the importance of different predictors in predicting stormflow volumes calculated by taking the median of the feature importance obtained for the basins belonging to the different classes: 6 refers to maximum importance, 1 to minimum importance.

features, suggests that, at the examined scales, our conclusions are generally relevant for Europe and its main climate regions.

5. Summary and conclusions

Understanding basin response to precipitation is crucial for flood forecasting, hydrological data assimilation, hydrological model calibration, and for better predicting the impact of climate change on future floods. In this study, we carried out a large-scale analysis considering 284 basins located in different regions of Europe. We extracted more than 60000 flood events that occurred in the period 1980–2015, and studied the coupling strength between *RC* and different proxies of pre-storm conditions (namely, antecedent precipitation index, surface and root zone soil moisture derived from hydrological, land surface model ingesting satellite surface soil moisture observations and reanalysis, pre-storm river discharge, snow water equivalent, and total water storage anomalies). We classified the 284 basins into five classes based on land cover and soil, long term climate, topography, and hydrological signatures: (i) Class 1, mountainous basins, (ii) Class 2, typically Mediterranean basins; (iii) Class 3, cold flat basins with high baseflow, (iv) Class 4, temperate/cold basins characterized by flashier behavior and impervious surfaces, (v) Class 5, cold basins characterized by a high fraction of pervious surfaces.

We found that, in Europe, precipitation explains relatively well the event water volume for both small and large events but not very well the event water peak discharge, especially for large flood events. The five classes of basins show different *RC* distributions, that generally correlates well with deep soil storages (such as root-zone soil moisture and pre-storm total water storage anomalies), pre-storm river discharge, and pre-storm snow water equivalent. In particular, across cold and mountainous regions, the snow water equivalent prior to the events plays a key role in controlling *RC* (see Section 4.3) and stormflow volume generation (Section 3.4), especially during spring and summer. Conversely, across warmer and more arid regions, deep pre-storm soil storages and pre-storm river discharge explain better *RC* variability. Poor correlations are found against antecedent precipitation index. This is a caveat to the hydrological community, that makes large use of this proxy.

Seasonal and interannual climate variability exert a key role on the coupling strength between *RC* and pre-storm conditions. For instance, unlike all the other classes, warmer basins (Class 2) show good correlations between pre-storm proxies and runoff coefficient also during the winter and for relatively wet periods. Conversely, for all the other classes, during the winter and during wet periods these correlations tend to decrease and peak during fall and relatively dry periods. While snow exerts an important role during spring time only for very cold basins, deep pre-storm soil storage are best correlated with *RC* especially during fall. Surface soil moisture storages exhibits stronger importance during summertime than wintertime. This data-driven multi-basin and multi-climate study examines the

ability of different pre-storm proxies to predict *RC* variability across a set of European basins. These results should be further explored within a large-scale soil moisture modeling, for example in land surface schemes, hydrological data assimilation studies, and generally in the design of flood forecasting systems. Our results indicate a possibly new evidence of strong climate/seasonal dependency on the coupling between pre-storm indices and *RC*, and also provide a new way to benchmark models and new observations in flood forecasting and climate studies — with the ultimate goal of improving our ability to make accurate assessments of future flood risks.

Open access data and code

- The precipitation, soil moisture, temperature and snow water equivalent (SWE) from ERA5 data used for the analysis are freely available via the Copernicus Climate Change Service (C3S) at https://cds.climate.copernicus.eu/cdsapp#!/dataset/reanalysis-era5-single-levels?tab=overview
- Discharge observations and shapefiles are obtained from the Global Runoff Data Center (GRDC, https://www.bafg.de/GRDC/EN/01_GRDC/grdc_node.html and are available under request https://www.bafg.de/GRDC/EN/01_GRDC/12_plcy/data_policy_node.html
- The soil moisture and evapotranspiration products of GLEAM 3.5a are accessible previous registration at https://www.gleam.eu
- SAC-SMA and SNOW17 models used for discharge simulations and soil moisture accounting are freely available https://github.com/danbroman/NWS_SacSMA_source. Potential evapotranspiration used within the SAC-SMA model was calculated with python pyet library https://github.com/phydrus/pyet while the routing functions can be downloaded here: https://github.com/chriscascia/hydrological_utilities. The calibration code is available via the pyswarm library here: https://pyswarms.readthedocs.io/en/latest/
- The regression analysis has been carried out with sci-kit python package available here: https://scikit-learn.org/stable/
- The code for the event extraction can be downloaded here: https://hydrograph-py.readthedocs.io/en/latest/index.html

CRediT authorship contribution statement

Christian Massari: Conceptualization, Methodology, Writing – original draft. **Victor Pellet:** Methodology, Writing – review & editing. **Yves Tramblay:** Methodology, Writing – review & editing. **Wade T. Crow:** Writing – review & editing. **Gaby J. Gründemann:** Data curation, Writing – review & editing. **Tristian Hascoetf:** Methodology, Writing – review & editing. **Daniele Penna:** Writing – review & editing. **Sara Modanesi:** Writing – review & editing. **Luca Brocca:** Writing – review & editing. **Stefania Camici:** Writing – review & editing. **Francesco Marra:** Conceptualization, Methodology, Writing – review & editing.

Declaration of competing interest

The authors declare that they have no known competing financial interests or personal relationships that could have appeared to influence the work reported in this paper.

Data availability

Data will be made available on request

Acknowledgments

CM, SM, LB and SC were supported by 4DMED-Hydrology European Space Agency project ESA 4D-MED (4000136272/21/I-EF) and DTE-Hydrology Evolution (4000136272/21/I-EF - CCN N. 1). FM was supported by the CARIPARO Foundation through the Excellence Grant 2021 to the "Resilience" Project. USDA ARS is an equal opportunity employer.

Appendix A. Supplementary data

Supplementary material related to this article can be found online at https://doi.org/10.1016/j.jhydrol.2023.130012.

References

Anon, 2020. Copernicus climate change service (C3S) ERA5: Fifth generation of ECMWF atmospheric reanalyses of the global climate. copernicus climate change service climate data store (CDS). URL: https://cds.climate.copernicus.eu/#!/search?text=ERA5&type=dataset.

Baker, D.B., Richards, R.P., Loftus, T.T., Kramer, J.W., 2004. A new flashiness index: Characteristics and applications to midwestern rivers and Streams1. JAWRA J. Am. Water Resour. Assoc. 40 (2), 503–522. http://dx.doi.org/10.1111/j.1752-1688.2004.tb01046.x, URL: https://onlinelibrary.wiley.com/doi/abs/10.1111/j.1752-1688.2004.tb01046.x. _eprint: https://onlinelibrary.wiley.com/doi/pdf/10.1111/j.1752-1688.2004.tb01046.x.

Bandhauer, M., Isotta, F., Lakatos, M., Lussana, C., Båserud, L., Izsák, B., Szentes, O., Tveito, O.E., Frei, C., 2021. Evaluation of daily precipitation analyses in E-OBS (V19.0e) and ERA5 by comparison to regional high-resolution datasets in European regions. Int. J. Climatol. 1 (21), http://dx.doi.org/10.1002/joc.7269, URL: https://onlinelibrary.wiley.com/doi/abs/10.1002/joc.7269.

Bauer-Marschallinger, B., Freeman, V., Cao, S., Paulik, C., Schaufler, S., Stachl, T., Modanesi, S., Massari, C., Ciabatta, L., Brocca, L., Wagner, W., 2019. Toward global soil moisture monitoring with sentinel-1: Harnessing assets and overcoming obstacles. IEEE Trans. Geosci. Remote Sens. 57 (1), 520–539. http://dx.doi.org/10.1109/TGRS.2018.2858004, Conference Name: IEEE Transactions on Geoscience and Remote Sensing.

Baugh, C., De Rosnay, P., Lawrence, H., Jurlina, T., Drusch, M., Zsoter, E., Prudhomme, C., 2020. The impact of SMOS soil moisture data assimilation within the operational global flood awareness system (GloFAS). Remote Sens. 12 (9), 1490. http://dx.doi.org/10.3390/RS12091490, https://www.mdpi.com/2072-4292/12/9/1490/htm. https://www.mdpi.com/2072-4292/12/9/1490.

Beck, H.E., Zimmermann, N.E., McVicar, T.R., Vergopolan, N., Berg, A., Wood, E.F., 2018. Present and future Köppen-Geiger climate classification maps at 1-Km resolution. Sci. Data 5, 180214. http://dx.doi.org/10.1038/sdata.2018.214, arXiv:30375988. URL: https://www.ncbi.nlm.nih.gov/pmc/articles/PMC6207062/.

Berghuijs, W.R., Harrigan, S., Molnar, P., Slater, L.J., Kirchner, J.W., 2019. The relative importance of different flood-generating mechanisms across europe. Water Resour. Res. 55 (6), 4582–4593. http://dx.doi.org/10.1029/2019WR024841, https://onlinelibrary.wiley.com/doi/full/10.1029/2019WR024841. https://onlinelibrary.wiley.com/doi/abs/10.1029/2019WR024841. https://agupubs.onlinelibrary.wiley.com/doi/10.1029/2019WR024841.

Berghuijs, W.R., Slater, L.J., 2023. Groundwater shapes North American river floods. Environ. Res. Lett. 18 (3), 034043. http://dx.doi.org/10.1088/1748-9326/acbecc, Publisher: IOP Publishing.

Berghuijs, W.R., Woods, R.A., Hutton, C.J., Sivapalan, M., 2016. Dominant flood generating mechanisms across the United States. Geophys. Res. Lett. 43 (9), 4382–4390. http://dx.doi.org/10.1002/2016GL068070, URL: https://onlinelibrary.wiley.com/doi/abs/10.1002/2016GL068070. _eprint: https://onlinelibrary.wiley.com/doi/pdf/10.1002/2016GL068070.

Bertola, M., Viglione, A., Vorogushyn, S., Lun, D., Merz, B., Blöschl, G., 2021. Do small and large floods have the same drivers of change? A regional attribution analysis in Europe. Hydrol. Earth Syst. Sci. 25 (3), 1347–1364. http://dx.doi.org/10.5194/hess-25-1347-2021, URL: https://hess.copernicus.org/articles/25/1347/2021/. Publisher: Copernicus GmbH.

Betchold, M., Modanesi, S., Lievens, H., Baguis, P., Brangers, I., Carassi, A., Getirana, A., Gruber, A., Heyvaert, Z., Massari, C., Scherrer, S., Vannitsem, S., De Lannoy, G., 2023. Assimilation of Sentinel-1 backscatter into a land surface model with river routing and its impact on streamflow simulations in two Belgian catchments. (submitted for publication).

Borga, M., Boscolo, P., Zanon, F., Sangati, M., 2007. Hydrometeorological Analysis of the 29 August 2003 flash flood in the Eastern Italian Alps. J. Hydrometeorol. 8 (5), 1049–1067. http://dx.doi.org/10.1175/JHM593.1, URL: https://journals.ametsoc.org/view/journals/hydr/8/5/jhm593_1.xml. Publisher: American Meteorological Society Section: Journal of Hydrometeorology.

Breiman, L., 2001. Random forests. Mach. Learn. 45 (1), 5–32. http://dx.doi.org/10.1023/A:1010933404324.

Breinl, K., Lun, D., Müller-Thomy, H., Blöschl, G., 2021. Understanding the relationship between rainfall and flood probabilities through combined intensity-duration-frequency analysis. J. Hydrol. 602, 126759. http://dx.doi.org/10.1016/j.jhydrol.2021.126759, URL: https://www.sciencedirect.com/science/article/pii/S002216942100809X.

Brocca, L., Melone, F., Moramarco, T., Morbidelli, R., 2009. Antecedent wetness conditions based on ERS scatterometer data. J. Hydrol. 364 (1), 73–87. http://dx.doi.org/10.1016/j.jhydrol.2008.10.007, URL: https://www.sciencedirect.com/science/article/pii/S002216940800512X.

Burnash, R.J.C., 1995. The NWS river forecast system - Catchment modeling. In: Computer Models of Watershed Hydrology. pp. 311–366, URL: https://www.cabdirect.org/cabdirect/abstract/19961904770. Publisher: Water Resources Publications.

Camici, S., Ciabatta, L., Massari, C., Brocca, L., 2018. How reliable are satellite precipitation estimates for driving hydrological models: A verification study over the Mediterranean area. J. Hydrol. 563, 950–961. http://dx.doi.org/10.1016/J.JHYDROL.2018.06.067.

Castillo, V.M., Gómez-Plaza, A., Martınez-Mena, M., 2003. The role of antecedent soil water content in the runoff response of semiarid catchments: A simulation approach. J. Hydrol. 284 (1), 114–130. http://dx.doi.org/10.1016/S0022-1694(03)00264-6, URL: https://www.sciencedirect.com/science/article/pii/S0022169403002646.

Chen, F., Crow, W.T., Starks, P.J., Moriasi, D.N., 2011. Improving hydrologic predictions of a catchment model via assimilation of surface soil moisture. Adv. Water Resour. 34 (4), 526–536. http://dx.doi.org/10.1016/j.advwatres.2011.01.011, URL: https://www.sciencedirect.com/science/article/pii/S030917081100025X.

Crow, W.T., Chen, F., Reichle, R.H., Liu, Q., 2017. L band microwave remote sensing and land data assimilation improve the representation of prestorm soil moisture conditions for hydrologic forecasting. Geophys. Res. Lett. 44 (11), 5495–5503. http://dx.doi.org/10.1002/2017GL073642, URL: https://onlinelibrary.wiley.com/doi/abs/10.1002/2017GL073642. _eprint: https://onlinelibrary.wiley.com/doi/pdf/10.1002/2017GL073642.

Crow, W.T., Chen, F., Reichle, R.H., Xia, Y., 2019. Diagnosing Bias in modeled soil moisture/runoff coefficient correlation using the SMAP level 4 soil moisture product. Water Resour. Res. 55 (8), 7010–7026. http://dx.doi.org/10.1029/2019WR025245, URL: https://onlinelibrary.wiley.com/doi/abs/10.1029/2019WR025245.

Cutler, D.R., Edwards, Jr., T.C., Beard, K.H., Cutler, A., Hess, K.T., Gibson, J., Lawler, J.J., 2007. Random forests for classification in ecology. Ecology 88 (11), 2783–2792. http://dx.doi.org/10.1890/07-0539.1, URL: https://onlinelibrary.wiley.com/doi/abs/10.1890/07-0539.1.

De Santis, D., Biondi, D., Crow, W.T., Camici, S., Modanesi, S., Brocca, L., Massari, C., 2021. Assimilation of satellite soil moisture products for river flow prediction: An extensive experiment in over 700 catchments throughout Europe. Water Resour. Res. 57 (6), http://dx.doi.org/10.1029/2021WR029643, e2021WR029643. URL: https://onlinelibrary.wiley.com/doi/abs/10.1029/2021WR029643.

Do, H.X., Mei, Y., Gronewold, A.D., 2020. To what extent are changes in flood magnitude related to changes in precipitation extremes? Geophys. Res. Lett. 47 (18), http://dx.doi.org/10.1029/2020GL088684, e2020GL088684. URL: https://onlinelibrary.wiley.com/doi/abs/10.1029/2020GL088684. _eprint: https://onlinelibrary.wiley.com/doi/pdf/10.1029/2020GL088684.

Entekhabi, D., Njoku, E.G., O'Neill, P.E., Kellogg, K.H., Crow, W.T., Edelstein, W.N., Entin, J.K., Goodman, S.D., Jackson, T.J., Johnson, J., Kimball, J., Piepmeier, J.R., Koster, R.D., Martin, N., McDonald, K.C., Moghaddam, M., Moran, S., Reichle, R., Shi, J.C., Spencer, M.W., Thurman, S.W., Tsang, L., Van Zyl, J., 2010. The soil moisture active passive (SMAP) mission. Proc. IEEE 98 (5), 704–716. http://dx.doi.org/10.1109/JPROC.2010.2043918.

Gnann, S.J., Coxon, G., Woods, R.A., Howden, N.J.K., McMillan, H.K., 2021. TOSSH: A toolbox for streamflow signatures in hydrology. Environ. Model. Softw. 138, 104983. http://dx.doi.org/10.1016/j.envsoft.2021.104983, URL: https://www.sciencedirect.com/science/article/pii/S1364815221000268.

Grömping, U., 2009. Variable importance assessment in regression: Linear regression versus random forest. Amer. Statist. 63 (4), 308–319, arXiv:25652309. URL: http://www.jstor.org/stable/25652309.

Gründemann, G.J., p. d. u. family=Giesen, given=Nick, Brunner, L., p. d. u. family=Ent, given=Ruud, 2022. Rarest rainfall events will see the greatest relative increase in magnitude under future climate change. Commun. Earth Environ. 3 (1), 1–9. http://dx.doi.org/10.1038/s43247-022-00558-8, URL: https://www.nature.com/articles/s43247-022-00558-8.

Guastini, E., Zuecco, G., Errico, A., Castelli, G., Bresci, E., Preti, F., Penna, D., 2019. How does streamflow response vary with spatial scale? Analysis of controls in three nested Alpine catchments. J. Hydrol. 570, 705–718. http://dx.doi.org/10.1016/j.jhydrol.2019.01.022, URL: https://www.sciencedirect.com/science/article/pii/S0022169419300678.

Hersbach, H., Bell, B., Berrisford, P., Hirahara, S., Horányi, A., Muñoz-Sabater, J., Nicolas, J., Peubey, C., Radu, R., Schepers, D., Simmons, A., Soci, C., Abdalla, S., Abellan, X., Balsamo, G., Bechtold, P., Biavati, G., Bidlot, J., Bonavita, M., Chiara, G.D., Dahlgren, P., Dee, D., Diamantakis, M., Dragani, R., Flemming, J., Forbes, R., Fuentes, M., Geer, A., Haimberger, L., Healy, S., Hogan, R.J., Hólm, E., Janisková, M., Keeley, S., Laloyaux, P., Lopez, P., Lupu, C., Radnoti, G., Rosnay, P.d., Rozum, I., Vamborg, F., Villaume, S., Thépaut, J.-N., 2020. The ERA5 global reanalysis. Q. J. R. Meteorol. Soc. 146 (730), 1999–2049. http://dx.doi.org/10.1002/qj.3803, URL: https://rmets.onlinelibrary.wiley.com/doi/abs/10.1002/qj.3803. _eprint: https://rmets.onlinelibrary.wiley.com/doi/pdf/10.1002/qj.3803.

Hofstra, N., Haylock, M., New, M., Jones, P.D., 2009. Testing E-OBS European high-resolution gridded data set of daily precipitation and surface temperature. J. Geophys. Res.: Atmos. 114 (D21), http://dx.doi.org/10.1029/2009JD011799, URL: https://onlinelibrary.wiley.com/doi/abs/10.1029/2009JD011799.

Hong, Y., Adler, R.F., Hossain, F., Curtis, S., Huffman, G.J., 2007. A first approach to global runoff simulation using satellite rainfall estimation. Water Resour. Res. 43 (8), http://dx.doi.org/10.1029/2006WR005739, URL: https://onlinelibrary.wiley.com/doi/abs/10.1029/2006WR005739.

Ivancic, T.J., Shaw, S.B., 2015. Examining why trends in very heavy precipitation should not be mistaken for trends in very high river discharge. Clim. Change 133 (4), 681–693. http://dx.doi.org/10.1007/s10584-015-1476-1, URL: http://link.springer.com/10.1007/s10584-015-1476-1.

Kerr, Y.H., Waldteufel, P., Wigneron, J.-P., Martinuzzi, J., Font, J., Berger, M., 2001. Soil moisture retrieval from space: The Soil Moisture and Ocean Salinity (SMOS) mission. IEEE Trans. Geosci. Remote Sens. 39 (8), 1729–1735, Publisher: IEEE.

Kim, S., Zhang, R., Pham, H., Sharma, A., 2019. A review of satellite-derived soil moisture and its usage for flood estimation. Remote Sens. Earth Syst. Sci. 2 (4), 225–246. http://dx.doi.org/10.1007/s41976-019-00025-7.

Komma, J., Reszler, C., Blöschl, G., Haiden, T., 2007. Ensemble prediction of floods – catchment non-linearity and forecast probabilities. Nat. Hazards Earth Syst. Sci. 7 (4), 431–444. http://dx.doi.org/10.5194/nhess-7-431-2007, URL: https://nhess.copernicus.org/articles/7/431/2007/.

Kuentz, A., Arheimer, B., Hundecha, Y., Wagener, T., 2017. Understanding hydrologic variability across Europe through catchment classification. Hydrol. Earth Syst. Sci. 21 (6), 2863–2879. http://dx.doi.org/10.5194/hess-21-2863-2017, URL: https://hess.copernicus.org/articles/21/2863/2017/.

Kumar, S.V., Reichle, R.H., Koster, R.D., Crow, W.T., Peters-Lidard, C.D., 2009. Role of subsurface physics in the assimilation of surface soil moisture observations. J. Hydrometeorol. 10 (6), 1534–1547. http://dx.doi.org/10.1175/2009JHM1134.1, URL: https://journals.ametsoc.org/view/journals/hydr/10/6/2009jhm1134_1.xml.

Kundzewicz, Z.W., Robson, A.J., 2004. Change detection in hydrological records—a review of the methodology / Revue méthodologique de la détection de changements dans les chroniques hydrologiques. Hydrol. Sci. J. 49 (1), 7–19. http://dx.doi.org/10.1623/hysj.49.1.7.53993, Publisher: Taylor & Francis _eprint.

Li, M., Wu, P., Ma, Z., 2020. A comprehensive evaluation of soil moisture and soil temperature from third-generation atmospheric and land reanalysis data sets. Int. J. Climatol. 40 (13), 5744–5766. http://dx.doi.org/10.1002/joc.6549, URL: https://onlinelibrary.wiley.com/doi/abs/10.1002/joc.6549.

Liaw, A., Wiener, M., 2002. Classification and Regression by RandomForest, Vol. 2.

Lievens, H., Tomer, S.K., Bitar, A.A., Lannoy, G.J.D., Drusch, M., Dumedah, G., Franssen, H.J.H., Kerr, Y.H., Martens, B., Pan, M., Roundy, J.K., Vereecken, H., Walker, J.P., Wood, E.F., Verhoest, N.E., Pauwels, V.R., 2015. SMOS soil moisture assimilation for improved hydrologic simulation in the Murray Darling Basin, Australia. Remote Sens. Environ. 168, 146–162. http://dx.doi.org/10.1016/J.RSE.2015.06.025.

Lloyd, S., 1982. Least squares quantization in PCM. IEEE Trans. Inform. Theory 28 (2), 129–137. http://dx.doi.org/10.1109/TIT.1982.1056489.

Lu, J., Sun, G., McNulty, S.G., Amatya, D.M., 2005. A comparison of six potential evapotranspiration methods for regional use in the Southeastern United States1. JAWRA J. Am. Water Resour. Assoc. 41 (3), 621–633. http://dx.doi.org/10.1111/j.1752-1688.2005.tb03759.x, URL: https://onlinelibrary.wiley.com/doi/abs/10.1111/j.1752-1688.2005.tb03759.x. _eprint: https://onlinelibrary.wiley.com/doi/pdf/10.1111/j.1752-1688.2005.tb03759.x.

Mahdi El Khalki, E., Tramblay, Y., Massari, C., Brocca, L., Simonneaux, V., Gascoin, S., El Mehdi Saidi, M., 2020. Challenges in flood modeling over data-scarce regions: How to exploit globally available soil moisture products to estimate antecedent soil wetness conditions in Morocco. Nat. Hazards Earth Syst. Sci. 20 (10), 2591–2607. http://dx.doi.org/10.5194/nhess-20-2591-2020, URL: https://www.scopus.com/inward/record.uri?eid=2-s2.0-85090906896&doi=10.5194%2fnhess-20-2591-2020&partnerID=40&md5=8e11335157f81eb5a0bfcd7fa055cc93. tex.document_type: Article tex.source: Scopus.

Manfreda, S., Brocca, L., Moramarco, T., Melone, F., Sheffield, J., 2014. A physically based approach for the estimation of root-zone soil moisture from surface measurements. Hydrol. Earth Syst. Sci. 18 (3), 1199–1212. http://dx.doi.org/10.5194/hess-18-1199-2014, URL: https://hess.copernicus.org/articles/18/1199/2014/. Publisher: Copernicus GmbH.

Mao, Y., Crow, W.T., Nijssen, B., 2020. Dual state/rainfall correction via soil moisture assimilation for improved streamflow simulation: Evaluation of a large-scale implementation with soil moisture active passive (SMAP) satellite data. Hydrol. Earth Syst. Sci. 24 (2), 615–631. http://dx.doi.org/10.5194/hess-24-615-2020, URL: https://hess.copernicus.org/articles/24/615/2020/.

Marchi, L., Borga, M., Preciso, E., Gaume, E., 2010. Characterisation of selected extreme flash floods in Europe and implications for flood risk management. Flash Floods: Observations and Analysis of Hydrometeorological Controls, J. Hydrol. Flash Floods: Observations and Analysis of Hydrometeorological Controls, 394 (1), 118–133. http://dx.doi.org/10.1016/j.jhydrol.2010.07.017.URL: https://www.sciencedirect.com/science/article/pii/S0022169410004427,

Martens, B., Miralles, D.G., Lievens, H., van der Schalie, R., de Jeu, R.A.M., Fernández-Prieto, D., Beck, H.E., Dorigo, W.A., Verhoest, N.E.C., 2017. GLEAM v3: Satellite-based land evaporation and root-zone soil moisture. Geosci. Model Dev. 10 (5), 1903–1925. http://dx.doi.org/10.5194/gmd-10-1903-2017, URL: https://gmd.copernicus.org/articles/10/1903/2017/. Publisher: Copernicus GmbH.

Massari, C., Brocca, L., Barbetta, S., Papathanasiou, C., Mimikou, M., Moramarco, T., 2014. Using globally available soil moisture indicators for flood modelling in Mediterranean catchments. Hydrol. Earth Syst. Sci. 18 (2), 839–853. http://dx.doi.org/10.5194/hess-18-839-2014, URL: https://www.scopus.com/inward/record.uri?eid=2-s2.0-84896859292&doi=10.5194%2fhess-18-839-2014&partnerID=40&md5=ced2d3c4b59a1a71b1d2dd39da6d898a. tex.document_type: Article tex.source: Scopus.

Massari, C., Camici, S., 2020. Antecedent wetness conditions of European floods: A comprehensive study. In: IGARSS 2020 - 2020 IEEE International Geoscience and Remote Sensing Symposium. pp. 3935–3938. http://dx.doi.org/10.1109/IGARSS39084.2020.9324459, ISSN: 2153-7003.

McDonnell, J.J., 2009. Hewlett, J.D. and Hibbert, A.R. 1967: Factors affecting the response of small watersheds to precipitation in humid areas. In sopper, W.E. and Lull, H.W., Editors, Forest hydrology, New York: Pergamon Press, 275—90. Progr. Phys. Geogr. Earth Environ. 33 (2), 288–293. http://dx.doi.org/10.1177/0309133309338118.

McKee, T., Doesken, N., Kleist, J., 1993. The relationship of drought frequency and duration to time scales. In: Proceedings of the Eighth Conference on Applied Climatology. American Meteorological Society, pp. 179–184.

Melone, F., Corradini, C., Singh, V.P., 2002. Lag prediction in ungauged basins: An investigation through actual data of the upper Tiber River valley. Hydrol. Process. 16 (5), 1085–1094. http://dx.doi.org/10.1002/hyp.313, URL: https://onlinelibrary.wiley.com/doi/abs/10.1002/hyp.313.

Merz, R., Blöschl, G., 2009. A regional analysis of event runoff coefficients with respect to climate and catchment characteristics in Austria. Water Resour. Res. 45 (1), http://dx.doi.org/10.1029/2008WR007163.

Norbiato, D., Borga, M., Merz, R., Blöschl, G., Carton, A., 2009. Controls on event runoff coefficients in the Eastern Italian Alps. J. Hydrol. 375 (3), 312–325. http://dx.doi.org/10.1016/j.jhydrol.2009.06.044, URL: https://www.sciencedirect.com/science/article/pii/S0022169409003485.

Pedregosa, F., Varoquaux, G., Gramfort, A., Michel, V., Thirion, B., Grisel, O., Blondel, M., Prettenhofer, P., Weiss, R., Dubourg, V., Vanderplas, J., Passos, A., Cournapeau, D., Brucher, M., Perrot, M., Duchesnay, É., 2011. Scikit-learn: Machine learning in python. J. Mach. Learn. Res. 12 (null), 2825–2830.

Penna, D., Borga, M., Zoccatelli, D., 2013. 7.9 Analysis of flash-flood runoff response, with examples from major European events. In: Shroder, J.F. (Ed.), Treatise on Geomorphology. Academic Press, pp. 95–104. http://dx.doi.org/10.1016/B978-0-12-374739-6.00153-6, URL: https://www.sciencedirect.com/science/article/pii/B9780123747396001536.

Penna, D., Tromp-van Meerveld, H.J., Gobbi, A., Borga, M., Dalla Fontana, G., 2011. The influence of soil moisture on threshold runoff generation processes in an alpine headwater catchment. Hydrol. Earth Syst. Sci. 15 (3), 689–702. http://dx.doi.org/10.5194/hess-15-689-2011, URL: https://hess.copernicus.org/articles/15/689/2011/hess-15-689-2011.html. Publisher: Copernicus GmbH.

Penna, D., van Meerveld, H.J., Zuecco, G., Dalla Fontana, G., Borga, M., 2016. Hydrological response of an Alpine catchment to rainfall and snowmelt events. J. Hydrol. 537, 382–397. http://dx.doi.org/10.1016/j.jhydrol.2016.03.040, URL: https://www.sciencedirect.com/science/article/pii/S0022169416301457.

Pieper, P., Düsterhus, A., Baehr, J., 2020. A universal Standardized Precipitation Index candiyear distribution function for observations and simulations. Hydrol. Earth Syst. Sci. 24 (9), 4541–4565. http://dx.doi.org/10.5194/hess-24-4541-2020, URL: https://hess.copernicus.org/articles/24/4541/2020/.

Ponce, V.M., Hawkins, R.H., 1996. Runoff curve number: Has it reached maturity? J. Hydrol. Eng. 1 (1), 11–19. http://dx.doi.org/10.1061/(ASCE)1084-0699(1996)1:1(11), URL: https://ascelibrary.org/doi/10.1061/%28ASCE%291084-0699%281996%291%3A1%2811%29. Publisher: American Society of Civil Engineers.

Rasheed, Z., Aravamudan, A., Sefidmazgi, A.G., Anagnostopoulos, G.C., Nikolopoulos, E.I., 2022. Advancing flood warning procedures in ungauged basins with machine learning. J. Hydrol. 609, 127736. http://dx.doi.org/10.1016/J.JHYDROL.2022.127736, URL: https://linkinghub.elsevier.com/retrieve/pii/S0022169422003110.

Reager, J.T., Famiglietti, J.S., 2009. Global terrestrial water storage capacity and flood potential using GRACE. Geophys. Res. Lett. 36 (23), http://dx.doi.org/10.1029/2009GL040826, URL: https://onlinelibrary.wiley.com/doi/abs/10.1029/2009GL040826.

Reichle, R.H., Lannoy, G.J.M.D., Liu, Q., Ardizzone, J.V., Colliander, A., Conaty, A., Crow, W., Jackson, T.J., Jones, L.A., Kimball, J.S., Koster, R.D., Mahanama, S.P., Smith, E.B., Berg, A., Bircher, S., Bosch, D., Caldwell, T.G., Cosh, M., González-Zamora, A., Collins, C.D.H., Jensen, K.H., Livingston, S., Lopez-Baeza, E., Martínnez-Fernández, J., McNairn, H., Moghaddam, M., Pacheco, A., Pellarin, T., Prueger, J., Rowlandson, T., Seyfried, M., Starks, P., Su, Z., Thibeault, M., van der Velde, R., J., W., Wu, X., Zeng, Y., 2017. Assessment of the SMAP Level-4 Surface and Root-zone soil moisture product using in situ measurements. J. Hydrometeorol. 18 (10), 2621–2645. http://dx.doi.org/10.1175/JHM-D-17-0063.1, URL: https://journals.ametsoc.org/view/journals/hydr/18/10/jhm-d-17-0063_1.xml.

Rodriguez-Galiano, V.F., Ghimire, B., Rogan, J., Chica-Olmo, M., Rigol-Sanchez, J.P., 2012. An assessment of the effectiveness of a random forest classifier for land-cover classification. ISPRS J. Photogramm. Remote Sens. 67, 93–104. http://dx.doi.org/10.1016/j.isprsjprs.2011.11.002, URL: https://www.sciencedirect.com/science/article/pii/S0924271611001304.

Rodriguez-Galiano, V., Mendes, M.P., Garcia-Soldado, M.J., Chica-Olmo, M., Ribeiro, L., 2014. Predictive modeling of groundwater nitrate pollution using random forest and multisource variables related to intrinsic and specific vulnerability: A case study in an agricultural setting (Southern Spain). Sci. Total Environ. 476–477, 189–206. http://dx.doi.org/10.1016/j.scitotenv.2014.01.001, URL: https://www.sciencedirect.com/science/article/pii/S0048969714000102.

Rousseeuw, P.J., 1987. Silhouettes: A graphical aid to the interpretation and validation of cluster analysis. J. Comput. Appl. Math. 20, 53–65. http://dx.doi.org/10.1016/0377-0427(87)90125-7, URL: https://www.sciencedirect.com/science/article/pii/0377042787901257.

Shahrban, M., Walker, J.P., Wang, Q.J., Robertson, D.E., 2018. On the Importance of Soil Moisture in Calibration of Rainfall–Runoff Models: Two Case Studies, Vol. 63, No. 9. Taylor & Francis, pp. 1292–1312. http://dx.doi.org/10.1080/02626667.2018.1487560, URL: https://www.tandfonline.com/doi/abs/10.1080/02626667.2018.1487560.

Sharma, A., Wasko, C., Lettenmaier, D.P., 2018. If precipitation extremes are increasing, why aren't floods? Water Resour. Res. 54 (11), 8545–8551. http://dx.doi.org/10.1029/2018WR023749, URL: https://onlinelibrary.wiley.com/doi/abs/10.1029/2018WR023749.

Simas, M., 1996. Lag Time Characteristics in Small Watersheds in the United states (Ph.D. thesis).

Sivapalan, M., Blöschl, G., Merz, R., Gutknecht, D., 2005. Linking flood frequency to long-term water balance: Incorporating effects of seasonality. Water Resour. Res. 41 (6), http://dx.doi.org/10.1029/2004WR003439, URL: https://onlinelibrary.wiley.com/doi/abs/10.1029/2004WR003439.

Slater, L.J., Villarini, G., 2016. Recent trends in U.S. flood risk. Geophys. Res. Lett. 43 (24), 12,428–12,436. http://dx.doi.org/10.1002/2016GL071199, URL: https://onlinelibrary.wiley.com/doi/abs/10.1002/2016GL071199. _eprint: https://onlinelibrary.wiley.com/doi/pdf/10.1002/2016GL071199.

Stein, L., Clark, M.P., Knoben, W.J.M., Pianosi, F., Woods, R.A., 2021. How do climate and catchment attributes influence flood generating processes? A large-sample study for 671 catchments across the contiguous USA. Water Resour. Res. 57 (4), http://dx.doi.org/10.1029/2020WR028300, e2020WR028300. URL: https://agupubs.onlinelibrary.wiley.com/doi/abs/10.1029/2020WR028300.

Tapley, B.D., Bettadpur, S., Watkins, M., Reigber, C., 2004. The gravity recovery and climate experiment: Mission overview and early results. Geophys. Res. Lett. 31 (9), http://dx.doi.org/10.1029/2004GL019920, URL: https://agupubs.onlinelibrary.wiley.com/doi/abs/10.1029/2004GL019920. _eprint: https://agupubs.onlinelibrary.wiley.com/doi/pdf/10.1029/2004GL019920.

Tarasova, L., Basso, S., Zink, M., Merz, R., 2018. Exploring controls on rainfall-runoff events: 1. Time series-based event separation and temporal dynamics of event runoff response in Germany. Water Resour. Res. 54 (10), 7711–7732. http://dx.doi.org/10.1029/2018WR022587, https://onlinelibrary.wiley.com/doi/full/10.1029/2018WR022587. https://onlinelibrary.wiley.com/doi/abs/10.1029/2018WR022587. https://agupubs.onlinelibrary.wiley.com/doi/10.1029/2018WR022587.

Tramblay, Y., Bouvier, C., Martin, C., Didon-Lescot, J.-F., Todorovik, D., Domergue, J.-M., 2010. Assessment of initial soil moisture conditions for event-based Rainfall–Runoff modelling. J. Hydrol. 387 (3), 176–187. http://dx.doi.org/10.1016/j.jhydrol.2010.04.006, URL: https://www.sciencedirect.com/science/article/pii/S0022169410001873.

Vaittinada Ayar, P., Mailhot, A., 2021. Evolution of Dry and wet spells under climate change over North-Eastern North America. J. Geophys. Res.: Atmos. 126 (5), http://dx.doi.org/10.1029/2020JD033740, e2020JD033740. URL: https://onlinelibrary.wiley.com/doi/abs/10.1029/2020JD033740.

Viglione, A., Merz, R., Blöschl, G., 2009. On the role of the runoff coefficient in the mapping of rainfall to flood return periods. Hydrol. Earth Syst. Sci. 13 (5), 577–593. http://dx.doi.org/10.5194/hess-13-577-2009, URL: https://hess.copernicus.org/articles/13/577/2009/. Publisher: Copernicus GmbH.

Wasko, C., Nathan, R., Peel, M.C., 2020. Changes in antecedent soil moisture modulate flood seasonality in a changing climate. Water Resour. Res. 56 (3), http://dx.doi.org/10.1029/2019WR026300, URL: https://onlinelibrary.wiley.com/doi/abs/10.1029/2019WR026300.

Wu, S., Zhao, J., Wang, H., Sivapalan, M., 2021. Regional patterns and physical controls of streamflow generation across the conterminous United States. Water Resour. Res. 57 (6), http://dx.doi.org/10.1029/2020WR028086, e2020WR028086. https://onlinelibrary.wiley.com/doi/full/10.1029/2020WR028086. https://onlinelibrary.wiley.com/doi/abs/10.1029/2020WR028086. https://agupubs.onlinelibrary.wiley.com/doi/10.1029/2020WR028086.

Yair, A., Klein, M., 1973. The influence of surface properties on flow and erosion processes on debris covered slopes in an arid area. Catena 1, 1–18. http://dx.doi.org/10.1016/S0341-8162(73)80002-5, URL: https://www.sciencedirect.com/science/article/pii/S0341816273800025.

Zhang, Y., Wei, H., Nearing, M.A., 2011. Effects of antecedent soil moisture on runoff modeling in small semiarid watersheds of Southeastern Arizona. Hydrol. Earth Syst. Sci. 15 (10), 3171–3179. http://dx.doi.org/10.5194/hess-15-3171-2011, URL: https://hess.copernicus.org/articles/15/3171/2011/.

Zhao, L., Liu, C., Sobkowiak, L., Wu, X., Liu, J., 2019. A review of underlying surface parameterization methods in hydrologic models. J. Geogr. Sci. 29 (6), 1039–1060. http://dx.doi.org/10.1007/s11442-019-1643-9.

Zolina, O., Simmer, C., Belyaev, K., Gulev, S.K., Koltermann, P., 2013. Changes in the duration of European wet and dry spells during the last 60 years. J. Clim. 26 (6), 2022–2047. http://dx.doi.org/10.1175/JCLI-D-11-00498.1, URL: https://journals.ametsoc.org/view/journals/clim/26/6/jcli-d-11-00498.1.xml.